

Conceptual Design of a Deployable Vehicular Bridge Structure Using Shape and Geometric Optimization for Post Disaster Relief Applications

by

Diana Estrada

B.S. Civil Engineering
Florida International University, 2015

Submitted to the Department of Civil and Environmental Engineering in Partial Fulfillment of
the Requirements for the Degree of

Master of Engineering in Civil and Environmental Engineering
at the

MASSACHUSETTS INSTITUTE OF TECHNOLOGY

June 2018

© 2018 Massachusetts Institute of Technology. All rights reserved.

Signature redacted

Signature of Author: _____

Department of Civil and Environmental Engineering
May 11th, 2018

Signature redacted

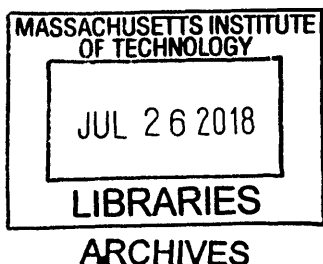
Certified by: _____

Josephine V. Carstensen
Lecturer of Civil Engineering and Environmental Engineering
Thesis Supervisor

Signature redacted

Accepted by: _____

Jesse Kroll
Professor of Civil and Environmental Engineering
Chair, Graduate Program Committee



Conceptual Design of a Deployable Vehicular Bridge Structure Using Shape and Geometric Optimization for Post Disaster Relief Applications

by

Diana Estrada

Submitted to the Department of Civil and Environmental Engineering
on May 11, 2018 in Partial Fulfillment of the
Requirements for the Degree of Master of Engineering in
Civil and Environmental Engineering.

In the aftermath of a natural disaster, all efforts are dedicated to a common goal: repairing and bringing the affected communities back to their fully functioning condition. However, it is frequently encountered that infrastructure and roads providing access to these communities are also damaged. As this can slow down the community response time significantly, there exists a need for light, easy to install, and effective temporary infrastructure for immediate restoration of communication.

This thesis presents a new design concept for a deployable bridge structure composed of scissor-like translational units. The proposed structure satisfies the deployment constraints and the stress limits determined by AASHTO LRFD Bridge Design Specifications. The used design approach uses multiple existing deployable geometries and performs a comparative analysis between the different systems. Given the particularity of SLE units, a standard finite element analysis method was enriched to match our conditions and enhance the accuracy of the modeling and analysis. This includes the implementation of master/slave node constraints and zero length rotational springs at the element nodes.

The design problem is formulated as a formal optimization problem with a nested equilibrium condition. Our objective function minimizes the total weight of the structure for a deployable bridge subjected to H15 design loads and stress limits delineated by AASHTO. A design exploration is performed to compare the best designs for different bridge geometries, angles of element inclination and member cross sectional areas. The optimization problem is solved using a genetic algorithm which, at each iteration, uses our beam finite element analysis to check that structural equilibrium is satisfied. Given the potential lack of resources after a natural disaster, providing a light weight extendible structure which would therefore require less force and resources for installation, can have a positive impact in the recovery process.

Thesis Supervisor: Josephine V. Carstensen
Title: Lecturer of Civil and Environmental Engineering

Acknowledgements

First and foremost, I would like to express my deepest gratitude to my thesis advisor, Josephine Carstensen. Her excitement, patience and wisdom has guided me not only through this thesis, but also through my time at MIT and professional path.

I would also like to thank our program advisor Gordana Herning for her assistance in helping me define the focus of my thesis and to Professor Jerome Connor for his guidance and expertise.

Next, I would like to express my appreciation for my friends and fellow M. Eng. classmates for the long work nights and endless encouragement. I am also deeply grateful for all the great people I have met at MIT, with whom I have created, and continue to create, great memories. Without their support and help, this thesis would have not been the same.

I would also like to thank my friends and family, near and far.

Most importantly, I would sincerely like to thank my parents for their unconditional support and encouragement to pursue my dreams, no matter what they are.

Table of Contents

Chapter 1 Introduction	9
1.1 Introduction.....	9
1.2 Research Objective.....	14
Chapter 2 Bridges for Disaster Relief and Basis for Design	15
2.1 Existing Types of Deployable Bridge Structures.....	15
2.2 Literary Review.....	17
2.3 Proposed Concept Design	20
2.4 Scissor Like Element Structures	20
Chapter 3 Design	23
3.1 Design Process	23
3.2 Design Parameters.....	25
Chapter 4 Geometric Design and Size Optimization	31
4.1 Design Approach.....	31
4.2 Geometric Design.....	31
4.3 Shape Optimization Problem Formulation.....	35
4.4 Optimization Problem Constraints	35
4.5 Optimization Methodology	39
4.6 Structural Analysis	40
Chapter 5 Results	45
5.1 Results	45
5.2 Discussion	55
Chapter 6 Conclusion	59
6.1 Summary of Findings.....	59
6.2 Future Work	60
References	61

List of Figures

Figure 1-Bridge failure by Hurricane Maria in Puerto Rico 2017, leaves communities without means of evacuation and means of communication for relief efforts [15] 10

Figure 2- Hito River Railroad Bridge collapse by flooding and scouring in Japan after Typhoon Nanmadol in 2012 [16] 10

Figure 3- Failure of steel truss bridge by Sumatra Earthquake and Tsunami in Indonesia 2004 [8] 10

Figure 4-Example of a deployable system, an umbrella, used regularly on a day to day basis, in its deployed and folded state [2]. 11

Figure 5-Classification of deployable structures based on the morphology and kinematic characteristics [10] 13

Figure 6- Geometric constitutive equation required for stress free SLE structures to be stress free in their deployed and folded condition. Reproduced from [3,6,37,38]..... 18

Figure 7- Single SLE unit displaying the location of angle θ_1 18

Figure 8- 2-D SLE model for a rectilinear translational geometry made out of wood coffee stirrers and staples. The image on the left shows the structure in its folded position. The image on the right, shows the structure in its deployed state at an arbitrary angle..... 20

Figure 9- Example of a two dimensional translational SLE unit consisting of two identical rigid beams jointed by a single pivot joint in the middle. 21

Figure 10-SLE basic unit types in the folded and deployed position: a)translational unit, b)polar unit, c) angulated unit [38]..... 22

Figure 11-Herein developed framework for the design and optimization of a deployable bridge structure. The framework is used for the design of the bridge structure in this study 24

Figure 12- Location of a bridge deck for a through bridge on a rectilinear translational SLE configuration..... 25

Figure 13-Location of bridge deck for a half-through bridge on a rectilinear translational SLE configuration with different member lengths. 26

Figure 14-AASHTO H-15 loading configuration. Adapted from [49]..... 27

Figure 15-Design parameters and loads used for the development of the proposed bridge, for a translational rectilinear bridge configuration..... 28

Figure 16-Supports and loading schematic for deployment check of the structure for pin-pin connection cantilever option 29

Figure 17-Range of the design domain for variable angles illustrated in a rectilinear translational geometry. All angles were evaluated for the three structure geometries proposed. 32

Figure 18- $T(1)$ structure geometry explored in bridge design. Rectilinear translational system composed of identical units with pivot points at the mid-point of each member. Geometry is derived from compatibility equations for translational units [38]. 33

Figure 19- $T(2)$ structure geometry explored in bridge design. Rectilinear translational system composed of SLE with different member lengths and pivot points at mid-points of each member. Bars of the same length run parallel to each other up to the mid-span. By mirroring the geometry along the y axis, an arch like structure is created. Geometry is derived from compatibility equations for translational units [38]..... 33

Figure 20- *T*(3) Structure geometry explored in bridge design defined as a rectilinear translational system composed of SLE units with different member lengths. Each unit is connected to a reverse configuration of itself, allowing bars of the same length to be connected to each other. Geometry is derived from compatibility equations for translational units [38]..... 34

Figure 21- Types of children created from generation to generation in a genetic algorithm [50]40

Figure 22- Isolated rigid bars which together create an SLE unit. Each rigid bar is composed of two independent elements rigidly joint together at the pivot point location (node 5 and 6) 41

Figure 23- Complete translational SLE unit, as modeled in the FE structural analysis MATLAB program. Rigid bars are connected to each other to form the SLE unit at the pivot joint location. 41

Figure 24- Master/slave node locations on coffee stirrer model of a rectilinear translational geometry *T*(2) with an arch like pattern..... 42

Figure 25- Common beam element modeled in finite element programs. This model assumes rigid connections [53]..... 43

Figure 26- Modified beam element with rotational springs for the modeling of semi-rigid or flexible connections [53]..... 43

Figure 27- External hinge locations on coffee stirrer model of a rectilinear translational geometry *T*(2) with an arch like pattern..... 44

Figure 28- Live load locations. Load case #4 resulted in the most critical loading location, figure 28(d)..... 45

Figure 29- Minimum weight solutions for all angles θ_1 in design domain for a *T*(1) geometry.. 47

Figure 30- Minimum weight solutions for all angles θ_1 in design domain for a *T*(2) geometry.. 48

Figure 31- Minimum weight solutions for all angles θ_1 in design domain for a *T*(3) geometry. 48

Figure 32-*T*(3)-B Geometry. Most optimal result based on minimum weight optimization objective..... 49

Figure 33-Maximum deflections vs. total weight relationship for the selected bridge geometries 51

Figure 34-Maximum bending moments vs. total weight relationship for the selected bridge geometries 51

Figure 35-Supports and loading schematic for deployability check of the structure for pin-pin connection cantilever option..... 53

Figure 36-Element bending moment during deployment for the *T*(3)-B bridge configuration... 53

Figure 37-Element internal forces during deployment for the *T*(3)-B bridge configuration..... 54

Figure 38-Problem solutions based on variable member length and deploy angle for a *T*(3)-B geometric configuration 55

Figure 39-Conceptual proposal for external locking mechanisms. SLE units on the left show the proposed locking member configuration in the folded position, whereas units on the right show locking members on their final deployed position..... 57

List of Tables

Table 1 -Existing types of portable temporary bridges used for military and civilian applications. Support and line of communication bridges are modular bridges whereas the tactical bridges are deployable as defined in the context of this study [7,20-27]	16
Table 2 - Design dead loads based on self-weight of structural and non-structural components and design live loads per AASHTO H-15 loading configurations [19]	27
Table 3 - 6061-T61 Aluminum Alloy Material Properties [19].....	29
Table 4 -Bridge designations based on SLE geometry and bridge deck location.....	34
Table 5 - Resultant deployed angle for the most optimal SLE structural performance per geometry as defined in section 4.2.....	47
Table 6 -Lowest cross sectional area solutions and objective function values for all geometries	49
Table 7 - Resultant forces and deflections for all selected geometries	50
Table 8 -Maximum member forces and deflections under deployment support conditions at the critical location.....	52
Table 9 -Design comparison with existing bridge designs. [25,46].....	57

Chapter 1 Introduction

1.1 Introduction

In the aftermath of a natural disaster, all efforts are dedicated to a common goal: repairing and bringing the affected communities back to their fully functioning condition. However, it is frequently encountered that infrastructure and roads providing access to these communities are also damaged, complicating the restoration activities. Therefore, deployable infrastructure, which can provide means of communication to the affected areas in a rapid manner, is vital for an efficient post disaster relief effort.

Preliminary reports of the infrastructure damages caused by hurricane Maria in 2017 state that approximately 18 bridges in Puerto Rico (Figure 1) were destroyed [1]. Immediate relief including the distribution of supplies and the restoration of power was delayed due to the inaccessibility to the affected locations. Similarly, other natural disasters such as landslides, earthquakes, flooding and tsunamis have caused significant damage to infrastructure. For example, In Indonesia, several bridges were destroyed and swept away by the 2004 Great Sumatra Earthquake and Indian Ocean Tsunami, leaving many small communities isolated (Figure 3) [2]. In Japan and Italy flooding caused bridges along the Hito River and the Po River respectively, to collapse (Figure 2) [3,4]. In 2010, 14 bridges collapsed in Chile as a result of the Maule earthquake. Deployable temporary bridges were installed to maintain lines of communication, while new permanent bridges were being designed under new earthquake codes [5]. These few examples, give an idea of the large degree of devastation caused by various natural disaster events, how disaster relief is a common need throughout the world, and how deployable structures can potentially be of use.



Figure 1- Bridge failure by Hurricane Maria in Puerto Rico 2017, leaves communities without means of evacuation and means of communication for relief efforts [6]



Figure 2- Hito River Railroad Bridge collapse by flooding and scouring in Japan after Typhoon Nanmadol in 2012 [7]



Figure 3- Failure of steel truss bridge by Sumatra Earthquake and Tsunami in Indonesia 2004 [2]

Furthermore, although the need for post disaster relief may increase due to the expected increase in natural and manmade disasters [8], there is very little research on the modification, or improvement of the existing temporary bridge designs. At the moment, the majority of these were designed in the mid-20th century by the military, for military loading requirements [8-10]. These bridges, although reliable, when used for civilian applications, are subjected to smaller load conditions and therefore are conservative. Developing a bridge design which would serve the load conditions specifically required for civilian applications, can potentially provide an alternative system which is lighter and more efficient.

While the main motivation for this research is the use of deployable structures for immediate relief, there exists the potential of using the design process and concept for other applications. Examples of these are: scaffolding, temporary infrastructure for construction access, and temporary supports for new infrastructure.

A deployable structure is one that can volumetrically transform from a compact state, to a larger deployed state when energy is applied to it [11]. Deployable structures are versatile systems with uses in diverse fields, often for their storage and transportation benefits. A familiar example of a deployable system is the umbrella (Figure 4). Umbrellas have the ability to be folded when not in use and transformed to a larger system after a force is applied.



Figure 4-Example of a deployable system. an umbrella, used regularly on a day to day basis, in its deployed and folded state [12].

On a larger scale, deployable structures are used on applications ranging from temporary architectural and civil structures to space applications [13,14]. Examples of these include: deployable shelters, roofs for stadiums, temporary stages, scissor lifts, temporary bridges, solar space arrays and deployable space antennas [11,13,15,16]. The structures need to meet two different equilibrium requirements: one when they are folded, and one when they are expanded static load bearing systems during operations. Moreover, a deployable structure must also be capable of performing as a reliable kinematic system while it deploys.

Deployable bridge structures provide a solution to post disaster relief efforts. Due to their transportability and ease of installation, they can be in service at the affected locations within a relatively short timeframe [8]. As such, they have been used for temporary lines of communication and have also been used for military applications throughout the world [2,8,5]. This thesis studies deployable bridges as temporary infrastructure and presents a new alternative design for post disaster relief applications.

Deployable structures have been classified according to their morphology and kinematics, by Hanour and Levy [17] (Figure 5). For this research, we will focus on a deployable structure that belongs to the pantographs (scissor) structures subcategory. Scissor structures can be deployed by the application of a single point force, which is beneficial given the possibility of lack of resources after an event. Also, these structures have high reliability during deployment and a large volume ratio between their stowed and deployed states [14,18]. While many applications of scissor structures have been proposed, not many have been formalized and constructed due to the design complexity of the system for deployment [18].

Nevertheless, with the use of existing computational optimization methods, known deployable assembly geometries and finite element analysis, this research aims to design a light bridge structure constructed out of scissor like units (SLEs).


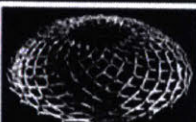




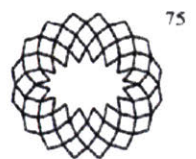
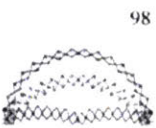



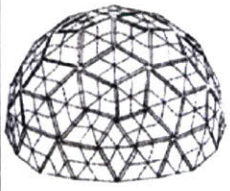
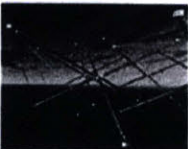
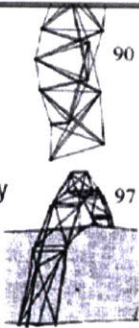



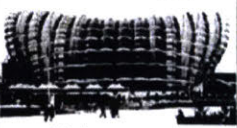
		Morphology			
		Lattice			Continuous
		DLG	SLG	Spine	Plates
		Pantographic (scissors)			Folded Plates
Kinematics	Rigid links	 Peripheral Scissors 19	 Angulated scissors (retractable roofs) 74	 Masts and arches 16	 Linear deployment 110
		 Radial scissors 22 55	 Others	 Reciprocal grids (Dismountable) 75	 Radial deployment 98
		Bars			Curved surface
		 Articulated joints 60	 Ruled surface 83	 Reciprocal grids (Dismountable) 85 93	 Curved surface 101
Deformable	Strut-cable systems		Tensioned membrane		
	 Tensegrity 68 69	 Others 90 97	 Fabric 120	 Hybrid 88	 Pneumatic Low pressure 124
			 Pneumatic High pressure		

Figure 5-Classification of deployable structures based on the morphology and kinematic characteristics [17]

1.2 Research Objective

The objective of this research is to introduce a new deployable bridge design for a short span structure aimed at immediate post disaster relief applications. With this in mind, the general design parameters to follow are: (i) geometry, (ii) weight, (iii) transportability, (iv) structural performance and (v) energy required for deployment. Specifically, the objective is to present a structural design which satisfies the deployment constraints and is optimized for minimum weight and subjected to the stress limits determined by AASHTO and deflection limits defined herein [19].

Chapter 2 Bridges for Disaster Relief and Basis for Design

2.1 Existing Types of Deployable Bridge Structures

For the purpose of this study a deployable structure is one that can volumetrically transform from a compact state, to a larger deployed state when energy is applied to it [11]. However, in literature the term “deployable structure” is used interchangeably to classify structures which are portable and rapid to install.

Deployable bridge structures, as defined in literature, have been designed and utilized since the beginning of the 20th century. Their research and implementation has mainly come from the military for combat and relief applications [8]. These bridges can be classified in three subcategories as used by the military: tactical, support and line of communication [20]. Table 1 summarizes these categories and provides a brief explanation of each. From the examples defined below, bridges on the support and line of communication categories are modular structures, whereas the tactical bridges are deployable. Although, the deployable bridges fall under the tactical classification, we would like to design one that is used as a line of communication. The extend of the bridge descriptions is only to provide a glimpse at the different available types. See references [8,20] for a complete description, history and field applications of the existing bridges.




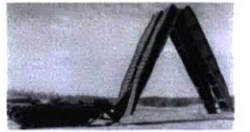




Category	Type	Description	Selected Span Length (ft)	Capacity at Selected Span Length	Image
Line of Communication	1-Bailey Bridge	Modular bridge. Composed of prefabricated truss members with pin connections. Bridge can be assembled in multiple heights and widths to allow for longer spans and higher load capacity.	60	MLC20 (SS) MLC75 (DS)	
	2-Acrow Bridge	Modular bridge. Composed of prefabricated truss members with pin connections. Similar to Bailey bridge however, the panels are taller. Also, bridge can have additional configurations and steel grades for longer spans and higher load capacity.	170	MLC120	
	3-Mabey Bridge	Similar system as the original Bailey design, but uses panels of different heights so that the final assembly would more closely resemble the bending moment diagram.	160	MLC80	
Tactical	4-Armor Vehicle Launched Bridges (AVLB)	Extendable bridge carried and installed by a vehicle launcher.	60	MLC70	
	5-Joint Assault Bridge (JAB)	Extendable bridge carried and installed by a vehicle launcher. Designed to eventually replace the AVLB.	60	MLC70	
	6-Wolverine	Extendable bridge carried and installed by a vehicle launcher. Designed to eventually replace AVLB and have higher load capacities.	78	MLC70	
Support	7-Medium Girder Bridge (MGB)	Modular bridge. Bridge is composed of a double girder and a bridge deck. It can be supported on unprepared ground. Bridge can be assembled in multiple heights and widths to allow for longer spans and higher load capacity.	62	MLC20 (SS) MLC70 (DS)	
	8-Dry Support Bridge	Modular bridge. Replacement to the MGB for support purposes, since it is a lighter bridge and allows for faster erection time.	66	MLC70	

Table 1-Existing types of portable temporary bridges used for military and civilian applications. Support and line of communication bridges are modular bridges whereas the tactical bridges are deployable as defined in the context of this study [8.20-27]

2.2 Literary Review

There exists in literature the study and proposal of alternative designs for deployable bridges additionally to those outlined in Table 1. Although these have concluded with promising results providing more efficient or lighter structures, to the best of the authors knowledge literature does not at current contain examples of actual applications.

Thrall et al. [28] have used structural optimization of panel topology, and of panel height and spatial orientation to present alternative designs for modular bridges. Also, different designs such as the Pratt truss, the bowstring truss, and network tied arches have also been proposed for modular construction [9]. Lederman et al. [29] presented a vehicular launched deployable bridge with a tied arch geometry, which has an unrolling deployment sequence. Another proposed patented design is the Mobile Bridge, which is a deployable structure composed of translational rectilinear SLE units. Full scale models and testing of the Mobile Bridge have been done and published [3,30,31]. Furthermore, there exists in literature various propositions of bridge concepts for military use, using alternative materials such as composites and FRP [32-36]. Most of the works in literature although characterized as easy to transport and install, still require onsite assembly and connections. In this study we propose a design which only requires the onsite expansion of a system which is fully assembled in its folded position.

Typically scissor like element (SLE) units are divided into three main geometries: translational, polar and angulated. These types will be described in detail in section 2.4. The main geometric relationship required for an SLE structure to be stress free in the deployed and folded condition is derived by Escrig [37] and referenced as the general deployability condition (equation 1). The equation states that the sum of the lengths of the members on each side of a unit line are equal to each other [3,6,37,38]. Unit lines are imaginary lines between one SLE unit and the other, which connect the upper and lower node of the scissor unit (shown as a dashed line in Figure 6)

$$a + b = c + d \quad [equation 1]$$

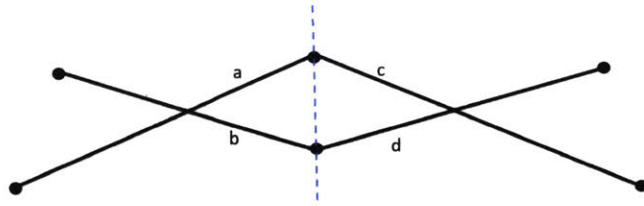


Figure 6- Geometric constitutive equation required for stress free SLE structures to be stress free in their deployed and folded condition. Reproduced from [13,16,37,38]

Based on derivations from the formula above Gantes [13], Escrig [37] and Maden et al. [38] provided guidelines and compatibility equations for the geometric design of stress free deployable structures. By varying the member lengths, the location of the pivot joint, and the modes of translation, [37,38] present a review of different scissor structural mechanisms which reliably provide deployment geometries. Additionally, Chikahiro et al. [3] explored the effects of geometric changes in the SLE structure's internal stresses by varying the angle of the diagonals. The study found that when θ_1 (Figure 7) is less than 30 degrees, the rate of increase of the member stresses is higher than the rate of increase at angles above 30 degrees. Our study seeks to compare the performance of the various SLE deployable system geometries in the context of a particular application, specifically, a bridge structure.

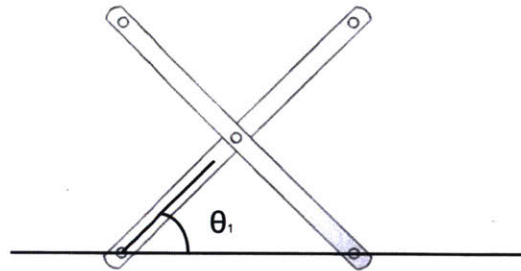


Figure 7- Single SLE unit displaying the location of angle θ_1

Alegria Mira and colleagues [14] compared the structural performance of all four scissor like element (SLE) unit types: translational, polar, angulated and USC. Translational, polar and angulated units are described in section 2.4. The USC is a recently developed scissor unit and is not studied in this thesis, further details can be found in [14]. Moreover, through a sensitivity analysis, they evaluated the effects of varying geometric properties in a system such as: thickness, height-span ratio and number of scissor units. This study found that the thickness of the element

is a very important parameter of the design. They also concluded that angulated units was the least efficient, where the USC performed the best under their design parameters. Furthermore, their results using a 2D linear elastic analysis matched the results of a 3D non-linear analysis of structures, therefore validating the use of the former as an approach for the design of these structures [15]. Gantes [13] and Pellegrino [6] studied the general field of deployable structures and their applications and, presented guidelines for the design and structural analysis of these. Gantes [3], Pellegrino [6] and Alegria Mira et al. [14] presented computational models of the SLE units. Furthermore, Alegria Mira et al. [14] used zero length rotational springs to model the hinges at the exterior nodes. Whereas, Gantes [13] and Pellegrino [16] presented the node/slave technique to represent the joint between the two diagonals that make up each SLE unit. The design approach presented herein proposes a simplified process which considers deployment reliability first.

Optimization methods have been used in the field to solve many problems. Gantes et al. [39] used the genetic algorithm (GA) to optimize for material and cross sectional properties of snap through deployable systems. You [40], used sequential quadratic programming to optimize for minimum weight or maximum stiffness in terms of geometry, cross sectional areas and materials [40]. Alegria Mira et al. [14] optimized arch geometries for deflections and structural performance using Rhinoceros' optimization plugin Karamba. Thrall et al. [41] used gradient-based steepest descent, GA, simulated annealing (SA) and damped least squares (DLS) to optimize the design of deployable structures composed of linkage elements. Also, Thrall et al. [9] used SA for minimum weight and maximum structural performance of modular bridges to find optimal length and form of panels. Additionally, on a single unit scale, Alegria Mira et al. [42] used a global shape optimization procedure for sizing, shape and structural optimization of a single unit to design the Universal Scissor Component.

The novelty of the study presented herein is the analysis and comparison of optimal SLE structures computed for various known deployable geometric configurations. At the same time, we incorporate into the shape optimization and geometric design exploration the allowable limits proposed by AASHTO, thus resulting in a concept which takes into account current code regulations. Moreover, this research presents a detailed design approach including the code variations required to properly model and analyze SLE deployable structures.

2.3 Proposed Concept Design

Following the design parameters outlined in section 1.3 of (i) geometry, (ii) weight, (iii) transportability, (iv) performance, and (v) energy required for deployment, we propose a deployable bridge design composed of SLE units. To form a structural system, the units are jointed to each other at their external top and bottom nodes to create a lattice. The bridge will be composed of two lattices which will be joint by transversal members supporting the deck.

During the initial exploration phase, small models were constructed to understand the behavior of SLE-type structures and to ensure that the geometry was feasible for our bridge application. The small scale models were built at MIT, using wood coffee stirrers for the rigid members and staples for the revolute joints and hinge connections. The lack of vertical and horizontal members, and the fact that the members in each unit are free to rotate at the hinge connections, allows the system to contract and expand. This characteristic, which facilitates transportability, makes SLE systems a great potential candidate for a deployable structure. An example of a lattice for the SLE bridge model in the deployed and extended condition is shown in Figure 8.

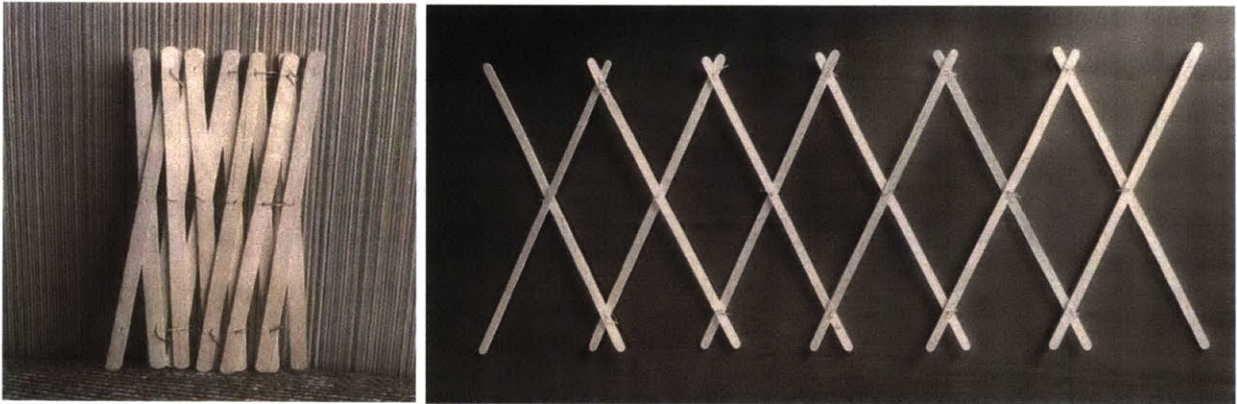


Figure 8- 2-D SLE model for a rectilinear translational geometry made out of wood coffee stirrers and staples. The image on the left shows the structure in its folded position. The image on the right, shows the structure in its deployed state at an arbitrary angle.

2.4 Scissor Like Element Structures

SLE units are structural units composed of two rigid members. The members are linked together by a common pivot joint, allowing independent rotations along the axis normal to their common plane (Figure 9) [5,13,38].

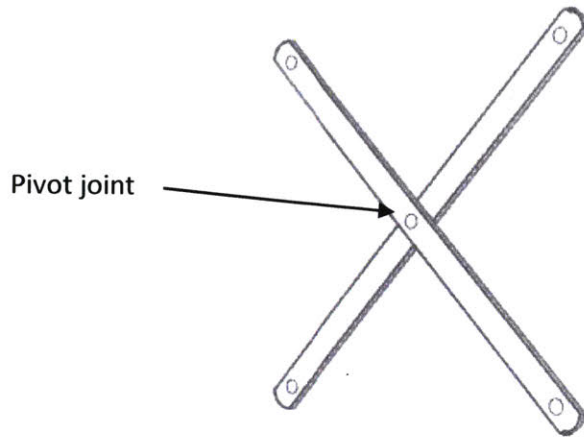
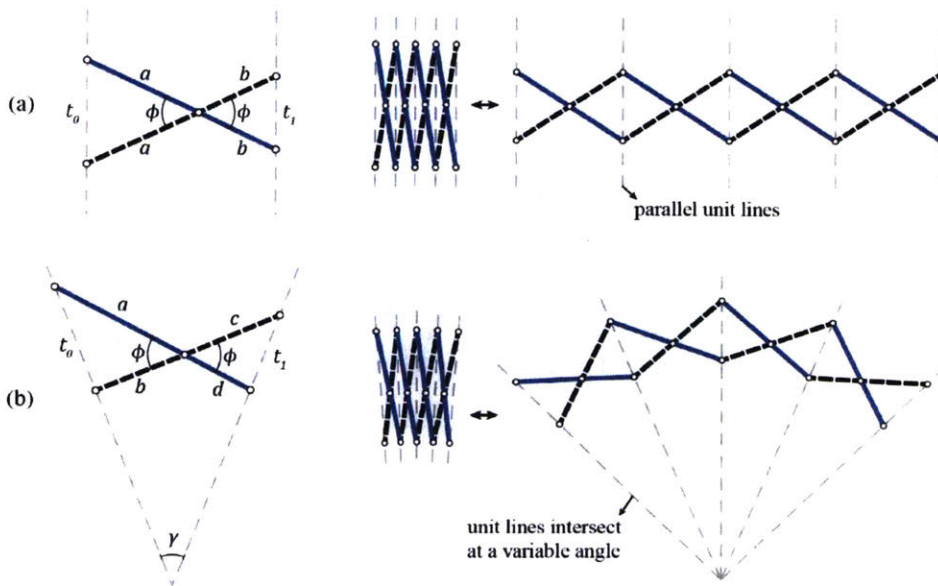


Figure 9- Example of a two dimensional translational SLE unit consisting of two identical rigid beams joined by a single pivot joint in the middle.

Based on the orientation of the unit lines and on the geometry, SLE's are categorized in three basic units: translational (Figure 10 a), polar (Figure 10 b), and angulated (Figure 10 c) [5,42,43]. Translational units, have two identical straight members and their pivot joint is in the middle of the member. When deployed, the unit lines are parallel to each other. Polar units, also have two identical straight members but the location of the pivot joint offset, creating a curvature during deployment. The unit lines meet at an angle γ which increases during deployment. Lastly, angulated units, are characterized by angled members which allow the structure to deploy in a radial configuration. The unit lines intersect at an angle γ which remains constant during deployment [5,42,43].



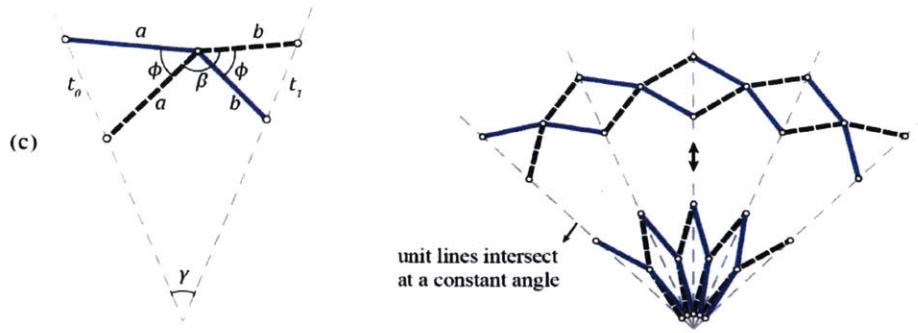


Figure 10-SLE basic unit types in the folded and deployed position: a)translational unit, b)polar unit, c) angulated unit [38]

Scissor structures can be formed by interconnecting SLE units together at their end points. When assembling these structures, geometric considerations must be carefully studied, not only to provide the desired final shape, but also to ensure a compatible and deployable system. Geometric compatibilities, which define the kinematic behavior and stresses during deployment, are dependent on the type of SLE unit selected and on the overall system geometry. When all the members of the structure fit together without deformations, i.e. without stresses, it is said that the structure is geometrically compatible. If this compatibility exists at all stages of deployment, then the structure is defined as *foldable* [44].

An essential geometric requirement for a stress free system is the general deployability condition shown in equation 1. Satisfying equation 1 ensures a stress free and compatible condition in the folded and deployed state for all members. It also ensures that when jointed together, SLEs create a system where all members in the linkage reach their most compact state at the same time. Thus, reducing the linkage theoretically to a single line, though discrete joint and member sizes dictate the actual size of the system [5,13,44].

However, this condition alone does not ensure geometric compatibility during deployment [16]. Additional considerations, as defined by Gantes and Maden et al., need to be satisfied to provide a stress free deployment, and therefore a foldable structure [13,38]. These conditions can be satisfied by following derived geometric and trigonometric equations which relate member lengths, symmetry, deployment angles, total span length and unit height. These equations, and the geometric systems reviewed by Maden et al. [38] are used in the development of the deployable bridge design described herein. It should be noted that a foldable structure, although stress free in the compact and deployed state, is not stable in the deployed state. Therefore, the system requires the addition of external locking mechanisms to create a rigid load bearing structure [13,44].

Chapter 3 Design

3.1 Design Process

The design process for a deployable structure is complex: it is a multistep iterative approach that requires both a detailed geometric analysis for deployment, and a structural analysis for stability at all stages of deployment, including of the folded and fully expanded states. Although the structure's behavior is usually linear in its deployed configuration, it is highly nonlinear and more complex during deployment. Therefore, it is generally recommended to first design the structure in its deployed configuration, and then check it for deployment stability [13, 16]. However, the design presented in this paper, as schematically illustrated in Figure 11, uses a simplified approach where we select an already deployable system as the basis for our design. To do so in an effective manner, our approach selects geometric systems which have already been proven to work for deployment based on a user defined SLE unit type. These, together with member cross sections, are provided as design variables for the structural analysis and optimization of the bridge in its deployed condition. The bridge geometry and member sizes are optimized for a minimum weight objective function. In this step, the structure is subjected to the parameters and loadings described in section 3.2. and designed to meet equilibrium requirements, stress limits as stipulated by AASHTO guidelines [19] and deflection limits as defined herein. Nevertheless, upon completion of the optimization and design in the deployed condition, the final configuration is checked to confirm deployment. The optimization scheme is described in detail in chapter 4.

Design and Optimization Process

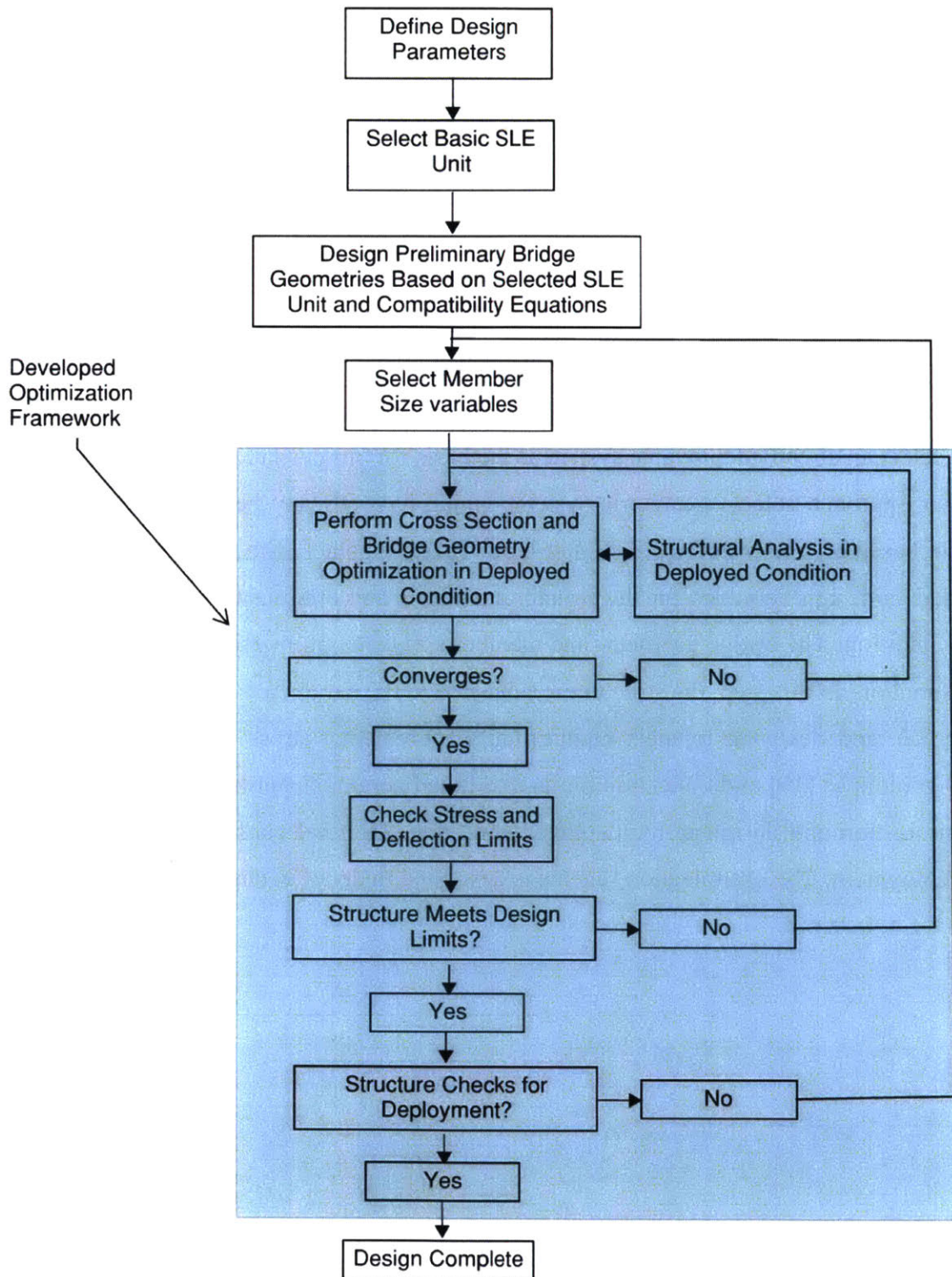


Figure 11-Herein developed framework for the design and optimization of a deployable bridge structure. The framework is used for the design of the bridge structure in this study

3.2 Design Parameters

The proposed bridge design is aimed at immediate post disaster relief applications. Therefore, the design parameters selected are based on the review of immediate needs after historical events and on previous studies into mobile structures. Specific needs for short span bridges for post disaster relief have been identified by the US Army in its Future Force Plan [29,35]. Furthermore, studies within the field often use short spans ranging from 50.00 ft up to 65.00 ft. Thus, to allow for comparison to previously design structures, a span length of 60 ft is selected [29,41,31,45]. The maximum member length has been selected based on transportation constraints. The US Department of Transportation imposes that vertical clearances for highways should be between 14.00 ft and 16.00 ft [46]. Considering the structure is being transported in a lowboy trailer, with an approximate height of 2.00 ft [47], a maximum member length of 12.00 ft is chosen. For geometries which have SLE units with different member lengths, a length of 11.00 ft is chosen for the shorter member, D_2 . Lastly, for material selection, aluminum alloy has been selected for the structural and non-structural components. Aluminum alloys provide high strength and a large stiffness to weight ratio. When compared to steel, aluminum alloys are approximately less than 1/4 of the weight yet as much as 1/3 of the stiffness. The lightness of the material is beneficial for the transportation and deployability of the system.

Another design variable explored is the location of the bridge deck. By varying the depth of the bridge deck we explore through (at SLE bottom) and half-through (at midpoint of SLE) bridge configurations as seen in Figure 12 and Figure 13, respectively.

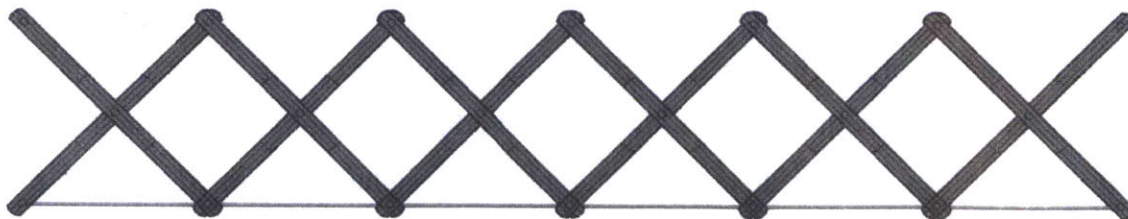


Figure 12- Location of a bridge deck for a through bridge on a rectilinear translational SLE configuration

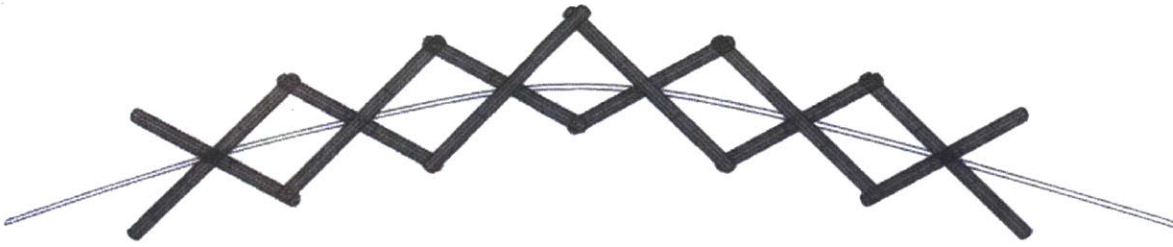


Figure 13-Location of bridge deck for a half-through bridge on a rectilinear translational SLE configuration with different member lengths.

The factored loads described in Table 2 have been applied to the structure in the locations shown in Figure 14. The bridge is being designed for AASHTO Strength I limit state with a load combination and load factors defined in equation 2.

$$L = \gamma_D(DL + SDL) + \gamma_L(LL) \quad \text{equation 2}$$

Where,

$$\gamma_D = \gamma_{D-max} = 1.25 \text{ for components and attachments} \quad [19]$$

$$\gamma_L = 1.75 \quad [19]$$

The dead load is being applied at the center of mass of each member, whereas the superimposed dead load is evenly distributed at all loading points. The live load selected is one of the design vehicle loads as specified by AASHTO Standard Specifications for Highway Bridges [48]. Although AASHTO specifies current bridge designs to use a higher design load than the one used in this study (H-20 vs. H-15), the lighter design load was selected based on the proposed bridge application. This load criterion allows for a line of communication, the passage of relief vehicles, civilian vehicles and supplies. The design vehicle load is applied as two point loads (Figure 14) and placed at different bridge locations to find the most critical position. The design live load is distributed to each of the adjacent load bearing points as a weighted function depending on the distance to each of the points.

Load	Load Description	Formulation
Dead Load	Self-weight	$DL = \sum_{e=1}^{nel} Lb^e * A^e * W_{Al}$
Super Imposed Dead Load	1 in Thick Aluminum Alloy Deck	$SDL = w_d * S * W_{Al}$
Live Load	H-15 Design Load (Figure 14)	$LL = 30,000 \text{ lbs}$

Where,

$$\begin{aligned}
 A^e &= \text{Cross - sectional area of each member} \\
 Lb^e &= \text{Length of each member} \\
 S &= \text{Length of bridge span} \\
 W_{Al} &= \text{unit weight of aluminum} = 0.1013 \text{ lb/in}^3 \\
 w_d &= \text{width of bridge deck} = 4 \text{ ft} \\
 S &= \text{Length of bridge span}
 \end{aligned}$$

Table 2- Design dead loads based on self-weight of structural and non-structural components and design live loads per AASHTO H-15 loading configurations [19]

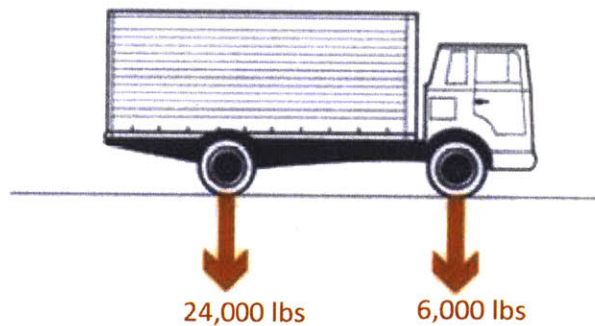


Figure 14-AASHTO H-15 loading configuration. Adapted from [49].

The design and loading parameters described above are shown in Figure 15 for an example of a translational rectilinear through bridge geometry. Additional bridge geometries will be studied in this work. Further details describing the different configurations are provided in chapter 4.

Design Parameters & Loading

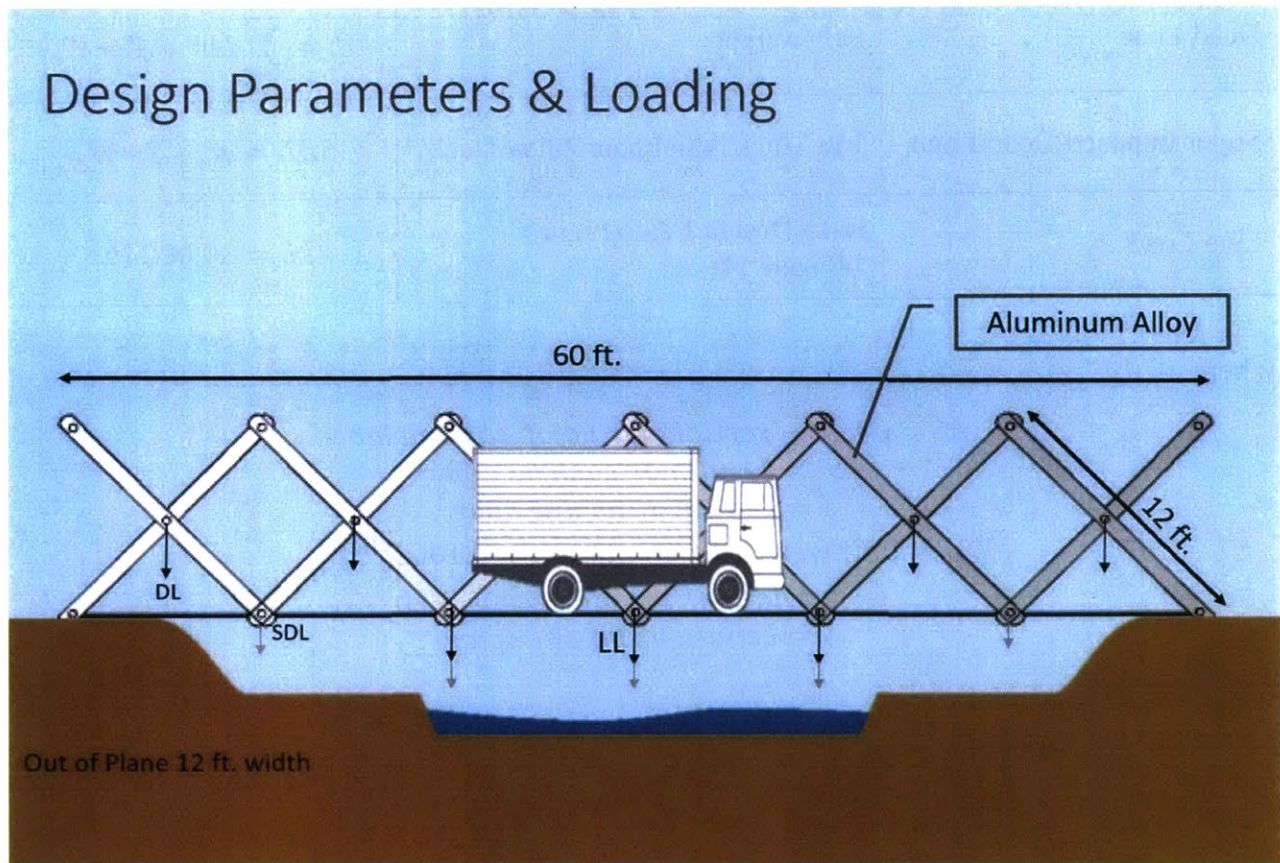


Figure 15-Design parameters and loads used for the development of the proposed bridge, for a translational rectilinear bridge configuration.

After the design of the bridge in the deployed condition, the structure is checked for deployment to ensure that the members do not exceed the allowable stresses and bending moments. For deployment analysis, the selected optimal bridge geometry is analyzed as a cantilever, assuming that the most critical condition is when the bridge is close to full deployment. That is, at an approximate 60-foot span, before reaching the end support. In this condition, the structure is subjected to its self-weight and the weight of the bridge deck (Figure 16). The top and bottom beam members of the lattice are fixed with rigid connections. Due to the higher complexity in the construction of fixed connections, we also analyzed the cantilever structures with pin-pin connections.

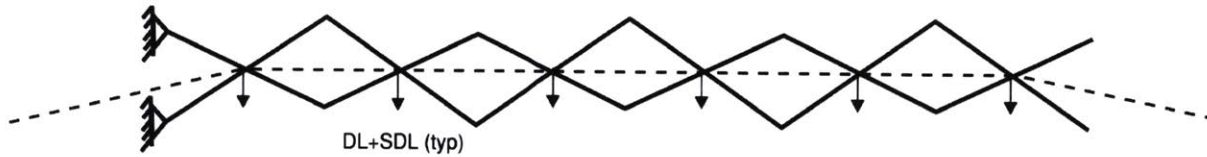


Figure 16-Supports and loading schematic for deployment check of the structure for pin-pin connection cantilever option

The material properties for the aluminum alloy selected for the design are outlined in Table 3 below, per AASHTO LRFD Bridge Design Specifications [19].

Aluminum Alloy Material Properties	
Specification	B209
Alloy-Temper	6061-T6, T651
Ultimate Tensile Strength (F_{tu})	42 ksi
Yielding Tensile Strength (F_{ty})	35 ksi
Ct (unwelded)	141
Compressive Yield Strength (F_{cy})	F_{ty}
Modulus of Elasticity (E)	10,100 ksi
Shear Modulus of Elasticity (G)	3,800 ksi
Poisson's ratio	0.33
Shear Yield Strength (F_{sy})	$0.6 * F_{ty}$
Shear Ultimate Strength (F_{su})	$0.6 * F_{tu}$

Table 3- 6061-T61 Aluminum Alloy Material Properties [19]

Chapter 4 Geometric Design and Size Optimization

4.1 Design Approach

A nested approach is proposed for the design problem which simultaneously explores the different geometric configurations and optimizes the member's cross sectional areas. The overall problem objective is to minimize the weight of the structure subject to deployability constraints, equilibrium, and stress and deflection limits. Through this approach, we aim to compute a solution which provides an optimal geometric and member size combination. Both the optimization formulation and geometric design are defined below.

The sizing optimization is defined as a formal optimization problem and solved using a constrained genetic algorithm with discrete variables. The design variables are the cross sectional depths and thicknesses and the sets of discrete options is defined by the user. The size optimization is performed simultaneously with the geometric design study. Since our approach has a low number of variables in the geometric design problem, it was computationally feasible to check all points in the design domain, thus ensuring a global optimal solution within the given domain.

4.2 Geometric Design

The first step for the geometric design of the structure is to define a SLE unit based on the design parameters. For this specific application, translational units were selected as the basic element of the system. Many of the studied structures in literature use translational units as their main design unit [13,44]. Comparatively, in previous research, angulated units proved to be the least efficient units for the studied structural systems [5]. Also, polar units create too large of a vertical curvature to be utilized as a bridge without additional considerations for the supports. Therefore, both, the angulated and the polar units were opted out of the design.

Once a design unit was selected, a variety of system geometries for this unit were explored. The selection of the proposed systems was done by choosing deployable SLE geometries for

translational units already presented in literature [38]. Based on their derived trigonometric and geometric equations for foldability, the structures were modified to meet our design criteria. Once selected, the translational geometries were defined within the model as a function $T(x)$ of predetermined nodal point locations, and are represented as $T(1)$, $T(2)$ and $T(3)$ which are discussed in detail below. The geometries were all evaluated by the structural analysis program and the size optimization scheme. Furthermore, all geometries were evaluated at various angles of deployment θ_1 , ranging from 24 to 46 degrees measured from the horizontal to the main diagonal (Figure 17).

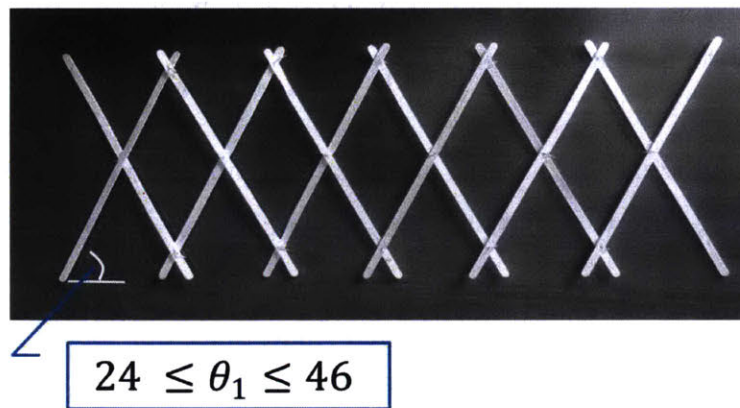


Figure 17-Range of the design domain for variable angles illustrated in a rectilinear translational geometry. All angles were evaluated for the three structure geometries proposed.

Through the design process, we computed and stored the optimized cross sections for all the different geometries in the design domain and subsequently compare them. The most optimal solution to our problem is a solution with the minimum weight across all geometries.

The three translational geometries $T(1)$, $T(2)$ and $T(3)$, are illustrated in Figure 18, Figure 19 and Figure 20 respectively. $T(1)$ defines a rectilinear translational geometry composed of identical members with pivot points at the mid-point of all elements. The pivot and external joints of each SLE lie on the same elevation with respect to each other (Figure 18).

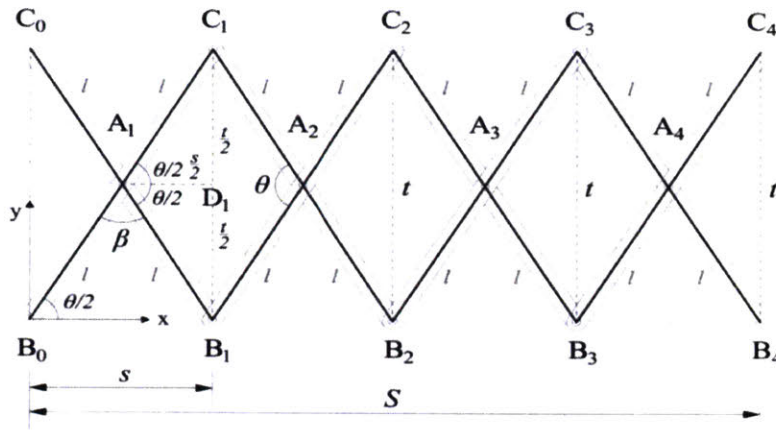


Figure 18- T(1) structure geometry explored in bridge design. Rectilinear translational system composed of identical units with pivot points at the mid-point of each member. Geometry is derived from compatibility equations for translational units [38].

T(2) is a rectilinear translational geometry composed of identical SLE units which have members of two different lengths. The members of equal length run parallel to each other and the pivot locations are at the mid-point of each element. The SLE units repeat identically up to the middle of the bridge span. The reverse configuration is then constructed thus creating an arch like structure, illustrated in Figure 19.

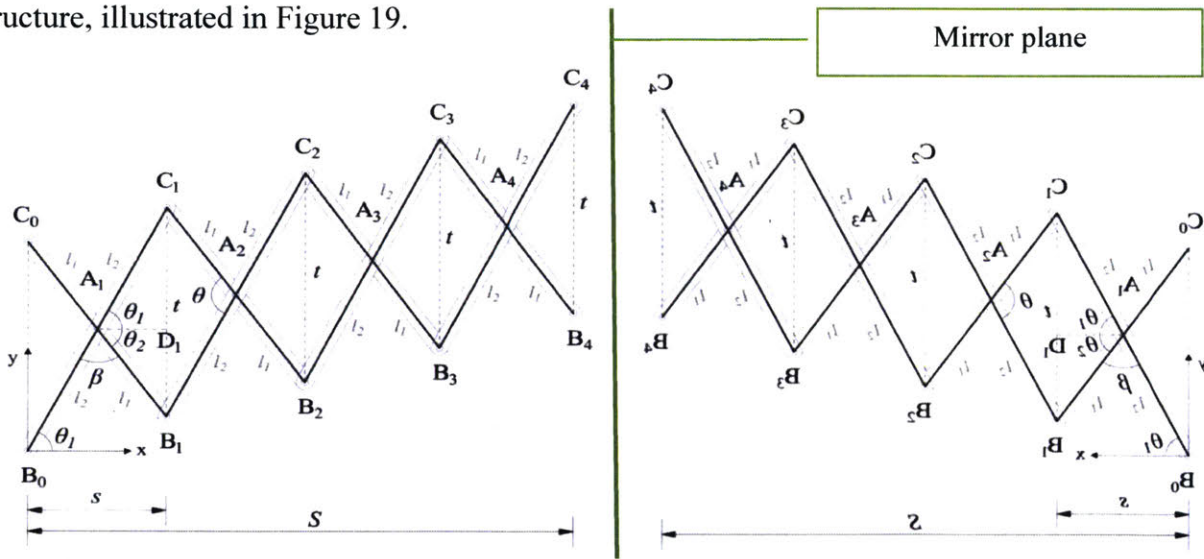


Figure 19- T(2) structure geometry explored in bridge design. Rectilinear translational system composed of SLE with different member lengths and pivot points at mid-points of each member. Bars of the same length run parallel to each other up to the mid-span. By mirroring the geometry along the y axis, an arch like structure is created. Geometry is derived from compatibility equations for translational units [38].

T(3) defines a rectilinear translational geometry composed of SLE units which have members of two different lengths. The SLE units are not repeated throughout the system. On the contrary, the lattice is constructed by joining an SLE with its reverse configuration. This causes, as illustrated

in Figure 20, members of the same length to be connected to each other. Though the revolute joints share the same elevation coordinate, the exterior hinges do not. This consideration is taken into account in the design by allowing the deck to be located in the middle of the structure as a half through bridge only.

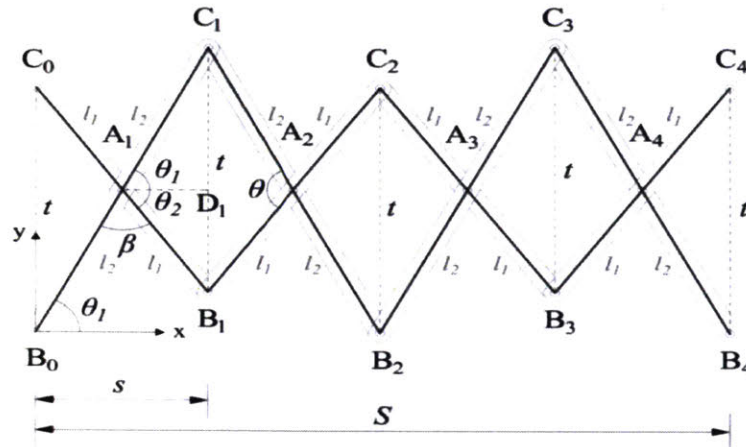


Figure 20- T(3) Structure geometry explored in bridge design defined as a rectilinear translational system composed of SLE units with different member lengths. Each unit is connected to a reverse configuration of itself, allowing bars of the same length to be connected to each other. Geometry is derived from compatibility equations for translational units [38].

By combining the three structure geometries along with the bridge deck depth variables, a total of 5 main configurations are studied. The configurations and their proposed designation for the purposes of this analysis are listed in Table 4.

Bridge Designation	SLE System Geometry	Bridge Type	Resultant
T(1)-A	T(1)	Through Bridge	
T(1)-B	T(1)	Half Through Bridge	
T(2)-A	T(2)	Through Bridge	
T(2)-B	T(2)	Half Through Bridge	
T(3)-B	T(3)	Half Through Bridge	

Table 4-Bridge designations based on SLE geometry and bridge deck location

4.3 Shape Optimization Problem Formulation

The objective of the shape optimization problem is to minimize the total weight of the structure subject to: the geometric layouts defined in the outer level, the stability of the structure and, the deflection and stress limits. The objective function is defined in equation 3 as follows:

$$\min_{A^e, e = 1 \dots nel} \quad h = \sum_{e=1}^{nel} Lb^e * A^e * W_{Al} \quad [\text{equation 3}]$$

Subject to

$$\mathbf{Kd} = \mathbf{F} \quad \text{Equilibrium}$$

$$c_1 \leq 0; \quad \text{for all } n = 1:nnp$$

$$c_2 \leq 0; \quad \text{for all } e = 1:nel$$

$$c_3 \leq 0; \quad \text{for all } e = 1:nel$$

$$c_4 \leq 0; \quad \text{for all } e = 1:nel$$

Where,

A^e = Cross – sectional area of the section

c_1 = Deflection limit

\mathbf{d} = Element displacent vector

\mathbf{F} = Element force vector

h = total weight of the structure

\mathbf{K} = Global stiffness matrix

Lb^e = length of each element

nel = Number of elements

nnp = Number of nodal points

W_{Al} = Unit weight of Aluminum

The constraints c_2, c_3, \dots, c_n are the design limits as stipulated by AASHTO [19] and will be described in detail in section 4.4 below.

4.4 Optimization Problem Constraints

The first design consideration in Eq. 4 is the equilibrium of the structure. It is calculated using a frame finite element analysis code. To meet equilibrium, the structure must satisfy equation 4. Details regarding this analysis are provided in section 4.6.

$$\mathbf{Kd} = \mathbf{F} \quad [\text{equation 4}]$$

AASHTO LRFD Bridge Design Specifications, contains no specific guidelines for temporary and/or deployable bridges and therefore M_{max} , F_{max} and V_{max} are calculated based on this code under Section 7, Aluminum Structures [33]. However, since the structure is not meant to be permanent, we have in this work calculated d_{max} as an average between the limits found in AASHTO and those found in literature for the design of similar bridges [19,35,45]. Stress and deflection limits are defined for each element and thus, all elements of the system must meet the defined constraints in Eq. 4.

The constraint c_1 ensures the deflection limits are satisfied. Deflection limits in literature range from Span/800, as defined by AASHTO [19] for permanent bridge structures, to Span/100 used by Bank and colleagues in the design of military deployable bridges [45].

Considering the proposed structure is being designed for temporary applications, a more flexible deflection limit d_{max} is defined as S/400. Thus, constraint c_1 is defined as follows :

$$c_1 = d_{max} - |d_n| \leq 0 \quad \text{[equation 5]}$$

Where,

$$\frac{S}{400} = d_{max}$$

$d_n = \text{node displacements}$
 $S = \text{Length of bridge span}$

The constraint c_2 restricts the maximum bending moment M_{max} . The maximum moment is calculated per AASHTO V7 section 7.11 [19].

$$c_2 = M_e - M_{max} \leq 0 \quad \text{[equation 6]}$$

Where,

$$M_{max} = \phi M_n$$

For which the reduction factors, $\phi = \phi_{ft} = 0.75$ for flexural tensile rupture and $\phi_f = 0.90$ for other flexural limits. Furthermore, the allowable bending moment, M_n , is calculated from the minimum value between, yielding flexural strength, rupture flexural strength and lateral torsional buckling.

$$M_n = \min \begin{cases} M_y \\ M_r \\ M_{tb} \end{cases} \begin{array}{l} \text{Yielding Flexural Resistance} \\ \text{Rupture Flexural Resistance} \\ \text{Lateral Torsional Buckling} \end{array}$$

The defined limits can be calculated per the equations found below.

$$\begin{aligned} M_y &= 1.3 * F_{cy} * S \\ M_r &= 1.42 * F_{tu} * S \\ M_{tb} &= F_{nb} * S; \end{aligned}$$

Where,

$$F_{nb} = \begin{cases} B_{br} - 2.3D_{br} \frac{d}{t} \sqrt{\frac{L_b}{C_b d}} & \text{if } \frac{d}{t} \sqrt{\frac{L_b}{C_b d}} < \frac{C_{br}}{2.3} \\ \frac{\pi^2 E}{5.29 \left(\frac{d}{t}\right)^2 \left(\frac{L_b}{C_b d}\right)} & \text{if } \frac{d}{t} \sqrt{\frac{L_b}{C_b d}} \geq \frac{C_{br}}{2.3} \end{cases}$$

$C_b = 1$ per section 7.10.2.2.3 [19]

D_{br}, C_{br}, B_{br} = buckling constants per table 7.5.4.3.2 [19]

d = cross-sectional depth

$L_b = Lb^e$ = unrestrained length of each element

M_e = maximum bending moment at each element due to applied loads.

t = cross-sectional thickness

The inequality constraint c_3 restricts the maximum allowable axial force F_{max} . It is calculated per reference [19], sections 7.8-7.9 as follows:

$$c_3 = |F_{ne}| - |F_{max}| \leq 0 \quad \text{[equation 7]}$$

The factored tensile resistance F_{max} shall be taken as ϕP_{nt} for which $\phi = \phi_y = 0.90$ for axial tension yielding and $\phi_u = 0.75$ for axial tension rupture. The nominal resistance P_n is the least of the nominal compressive resistance for tensile yielding and for tensile rupture which are represented and described below.

$$\begin{aligned} P_{nt} &= \min \begin{cases} P_y \\ P_u \end{cases} \begin{array}{l} \text{Tensile Yielding} \\ \text{Tensile Rupture} \end{array} \\ P_y &= F_{ty} * A \\ P_u &= F_{tu} * A \end{aligned}$$

The factored resistance for compression members F_{max} shall be taken as ϕP_n where $\phi = \phi_c = 0.90$ for axial compression. The nominal resistance P_n is the least compressive resistance of the following:

$$P_n = \min \left\{ \begin{array}{l} P_{mb} \\ P_{lb} \\ P_{m-lb} \end{array} \right\} \begin{array}{l} \text{Member Buckling} \\ \text{Local Buckling} \\ \text{Member and Local Buckling} \\ \text{Interaction} \end{array}$$

For which

$$P_{mb} = F_c * A$$

$$P_{lb} = \sum_{e=1}^{nel} F_{nce} A_e + F_{cy} (A_g - \sum_{e=1}^{nel} A_e)$$

$$P_{m-lb} = \begin{cases} \left[\frac{.85\pi^2 E}{\left(\frac{Kl}{r}\right)^2} \right]^{\frac{1}{3}} F_e^{\frac{2}{3}} A & \text{if } F_e < F_c \\ \min \{ P_{mb} \} & \text{otherwise} \end{cases}$$

Where,

$$F_c = \begin{cases} .85(B_c - D_c \frac{Kl}{r}) \leq F_{cy} & \text{if } \frac{Kl}{r} < C_c \\ \frac{.85\pi^2 E}{\left(\frac{Kl}{r}\right)^2} & \text{if } \frac{Kl}{r} \geq C_c \end{cases}$$

$$F_{nce} = \begin{cases} F_{cy} & \text{if } \frac{b}{t} \leq \frac{B_p - F_{cy}}{1.6D_p} \\ B_p - 1.6D_p \frac{b}{t} & \text{if } \frac{B_p - F_{cy}}{1.6D_p} \leq \frac{b}{t} \leq \frac{k_1 B_p}{1.6D_p} \\ \frac{k_2 \sqrt{B_p E}}{1.6 \frac{b}{t}} & \text{if } \frac{b}{t} \geq \frac{k_1 B_p}{1.6D_p} \end{cases}$$

$A = A_e = A_g$ = Cross-sectional area

$b = d$ = Cross-sectional depth

F_{ne} = maximum axial force at each element due to applied loads

F_e = Elastic buckling stress = $\frac{\pi^2 E}{(1.6b/t)^2}$ per table 7.5.4.9-1 [19]

D_c, C_c, B_c, D_p, B_p = buckling constants per table 7.5.4.3.2 [19]

$\frac{Kl}{r}$ = Effective slenderness of member

k_1, k_2 = Post buckling constant for flat elements

The inequality constraint c_4 defines the maximum shear resistance V_{max} . It is calculated as follows per section 7.10.3 [19]:

$$c_4 = V_e - V_{max} \leq 0 \quad \text{[equation 8]}$$

$V_{max} = \phi V_n$ where the reduction factor $\phi = \phi_s = 0.90$ for shear. The nominal shear resistance is calculated as follows:

$$V_n = F_{ns} * A$$

Where:

$$F_{ns} = \begin{cases} F_{sy} & \text{if } \frac{b}{t} \leq \frac{B_s - F_{sy}}{1.25D_s} \\ B_s - 1.25D_s \frac{b}{t} & \text{if } \frac{B_s - F_{sy}}{1.25D_s} \leq \frac{b}{t} \leq \frac{C_s}{1.25} \\ \frac{\pi^2 E}{(1.25b/t)^2} & \text{if } \frac{b}{t} \geq \frac{C_s}{1.25} \end{cases}$$

D_s, C_s, B_s = buckling constants per table 7.5.4.3.2 [19]

V_e = maximum shear force at each element due to applied loads.

4.5 Optimization Methodology

The sizing optimization problem is formulated as a constrained problem with discrete design variables. A MATLAB optimization program was written using the genetic algorithm *ga* function [44] which runs simultaneously with the bridge geometric exploration. The problem is constrained by structural stability and stress and deflection limits, therefore, a beam finite element analysis code (FEA) is nested into the GA optimizer for the analysis of the structure.

The genetic algorithm (GA) is a stochastic search method which solves constrained and unconstrained optimization problems. The algorithm is inspired on Darwin's theory of natural selection [41,50,51]. The GA starts with an initial random population, where each individual is evaluated on the objective function. Depending on the individual's performance, members of the first generation are selected as parents for a new generation. The next generation is created by a combination of the fittest members carried over from the previous generation, and of children created through mutations and crossovers of the selected parents. This combination provides a generation with a better average objective function. Crossover children are created by combining "chromosomes" from pairs of parents of the current generation, whereas children from mutations

are created by altering “genes” of individual parents [51]. Each generation is an iteration of the algorithm and continues from generation through generation until a stopping criterion is reached. Figure 21 provides a representation of the creation of children for the next generation through either elitism, crossover or mutation. GA is used in many fields including structural applications and sizing optimization. However, due to the nature of its random variable evaluation there is no guarantee the output solution is the globally optimal solution. To reduce the risk of converging to a bad local minima, the problem is evaluated multiple times and the result with the smallest area is selected as the most optimal result.

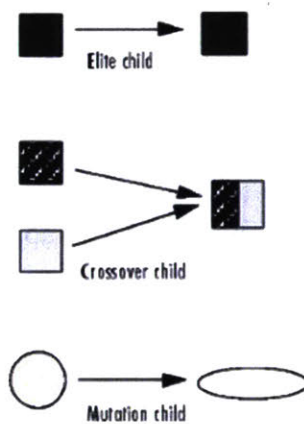


Figure 21- Types of children created from generation to generation in a genetic algorithm [50]

4.6 Structural Analysis

In an effort to have an efficient interface between the optimization program and the structural analysis program, the SLE structure is analyzed using a finite element method programmed in MATLAB [50]. Furthermore, the use of a MATLAB code for the structural analysis provides the ability to enrich the standard FEA to match the conditions of the deployable bridge. Therefore, special considerations are taken into account for the modeling and analysis of the structure. These include the proper element selection and discretization, as well as the appropriate end node behavior and connections. Review of a standard FEA frame analysis is beyond the scope of this thesis and the reader is referred to [53] for more information.

An SLE unit is composed of two independent rigid bars which have a node at their pivot point location as illustrated in Figure 22 and Figure 23. Each bar is modeled as two separate beam elements, and the node at the pivot point rigidly joins them together (nodes 5 & 6 in Figure 22).

For example, using the SLE unit in Figure 23, elements 1 and 4 are rigidly connected by node 5 and elements 2 and 3 by node 6. The rigid connection in a 2D plane, equates to all degrees of freedom (DOF) restrained; 2 translational DOFs and 1 rotational DOF. Furthermore, the two rigid bars are connected to each other at their pivot joint to form the SLE unit. To do so, using Figure 23 as an example, nodes 5 and 6 are collocated in the design plane and are related in translation by the master/slave node technique. This results in an approximate approach which models the SLE unit as four independent beam elements, with rigid connections along the bars at the mid nodes and pin connections at all the external joints (Figure 23) [5,13,16].

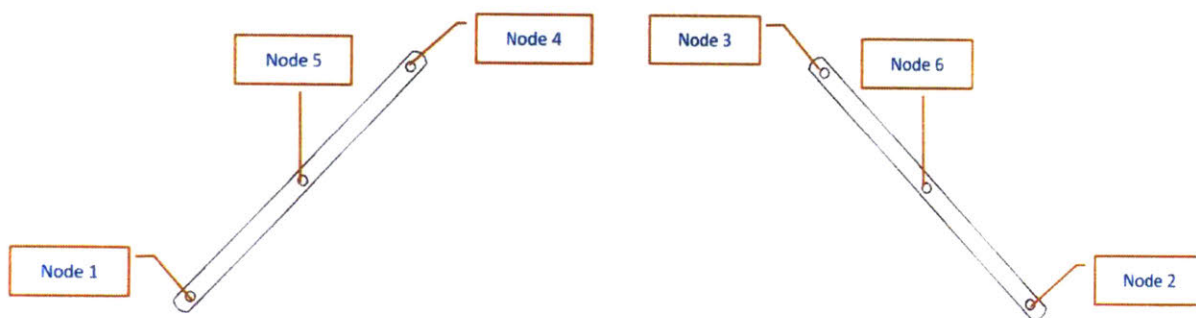


Figure 22- Isolated rigid bars which together create an SLE unit. Each rigid bar is composed of two independent elements rigidly joint together at the pivot point location (node 5 and 6)

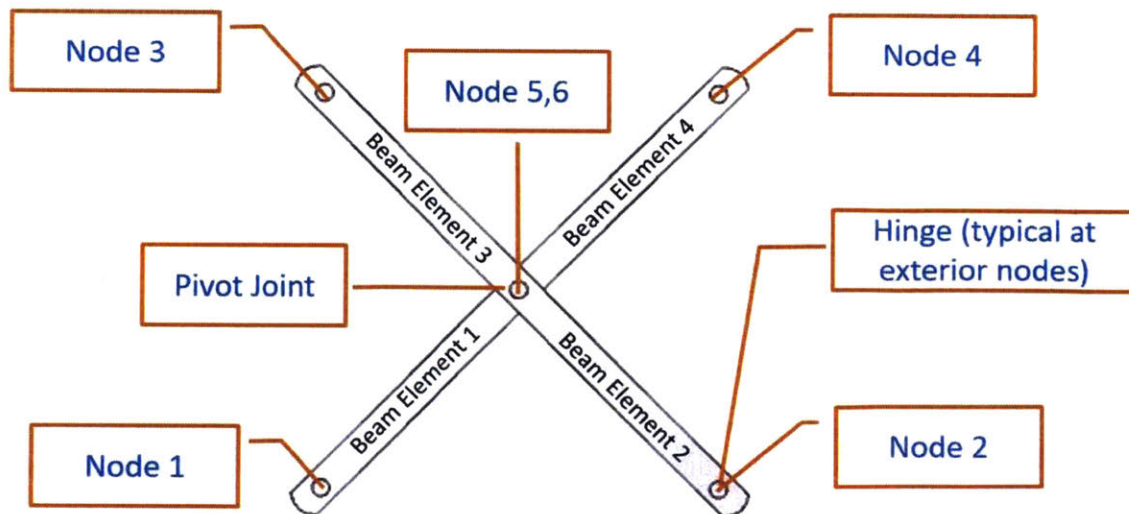


Figure 23- Complete translational SLE unit, as modeled in the FE structural analysis MATLAB program. Rigid bars are connected to each other to form the SLE unit at the pivot joint location.

The master/slave node (also called the parent-child method) relates two nodes together by constraining the displacement of one node (slave node) to be equal to the displacement of its master node [52]. In our analysis, the middle nodes of each bar are related to each other with the master/slave node condition to form an SLE unit (Figure 24). This technique creates a link between the bars by constraining the 2 translational DOFs. Nonetheless, the nodes are free to rotate about their common axis perpendicular to the plane.

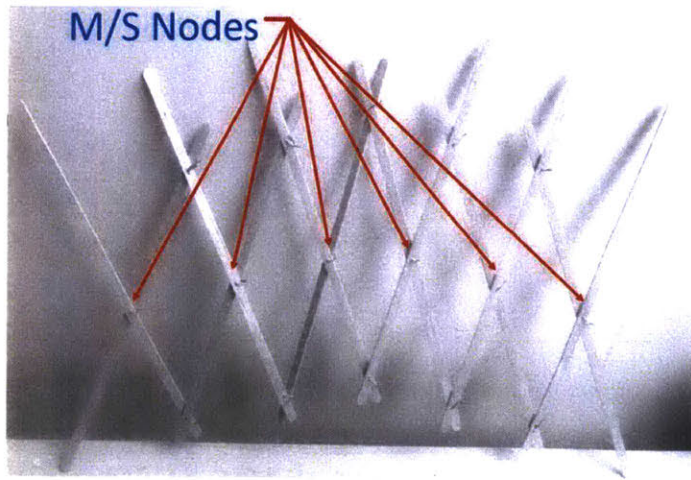


Figure 24-Master slave node locations on coffee stirrer model of a rectilinear translational geometry T(2) with an arch like pattern.

To enforce this relationship in the FEA program, the displacement vectors for the elements that have a slave node, are modified to reflect the displacement of the master node as follows:

Displacement vector for the SLE unit shown in Figure 23 without the master/slave condition

$$\begin{array}{cccc}
 x1 & x2 & x3 & x4 \\
 y1 & y2 & y3 & y4 \\
 \theta1 & \theta2 & \theta3 & \theta4 \\
 \mathbf{d}^{e1} = \begin{bmatrix} x5 \\ y5 \\ \theta5 \end{bmatrix} & \mathbf{d}^{e2} = \begin{bmatrix} x6 \\ y6 \\ \theta6 \end{bmatrix} & \mathbf{d}^{e3} = \begin{bmatrix} x5 \\ y5 \\ \theta5 \end{bmatrix} & \mathbf{d}^{e4} = \begin{bmatrix} x6 \\ y6 \\ \theta6 \end{bmatrix}
 \end{array}$$

Modified displacement vector for the SLE unit shown in Figure 23 with the master/slave node condition, assuming node 5 is the master node whereas node 6 is the slave node.

$$\begin{array}{cccc}
 x1 & x2 & x3 & x4 \\
 y1 & y2 & y3 & y4 \\
 \theta1 & \theta2 & \theta3 & \theta4 \\
 \mathbf{d}^{e1} = \begin{bmatrix} x5 \\ y5 \\ \theta5 \end{bmatrix} & \mathbf{d}^{e2} = \begin{bmatrix} x5 \\ y5 \\ \theta6 \end{bmatrix} & \mathbf{d}^{e3} = \begin{bmatrix} x5 \\ y5 \\ \theta5 \end{bmatrix} & \mathbf{d}^{e4} = \begin{bmatrix} x5 \\ y5 \\ \theta6 \end{bmatrix}
 \end{array}$$

Another important consideration required for the modeling of the SLE structure is the proper connection of SLE units to each other. The two rigid bars which make up the SLE unit are jointed to adjacent units with pin connections and do not carry a moment from bar to bar. Therefore, the external node connections must be properly modeled as flexible connections. Otherwise, assuming rigid connections at the outer nodes, overestimates the stiffness of the element and leads to inaccurate results. To approximate the connection flexibility in the analytical model, zero length rotational springs are added at the ends of the beam element as shown in Figure 26. Only the rotational stiffness along the axis perpendicular to the plane is considered with the addition of the springs, the other structural properties of the springs are not taken into account.

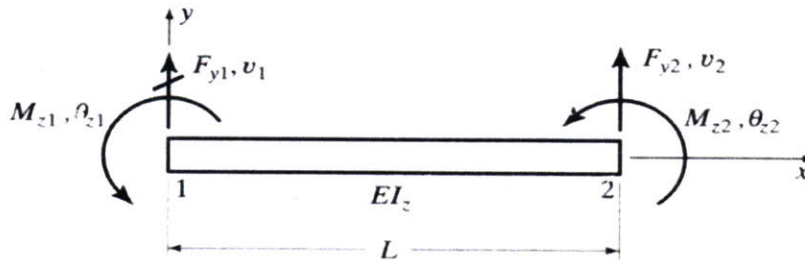


Figure 25-Common beam element modeled in finite element programs. This model assumes rigid connections [53]

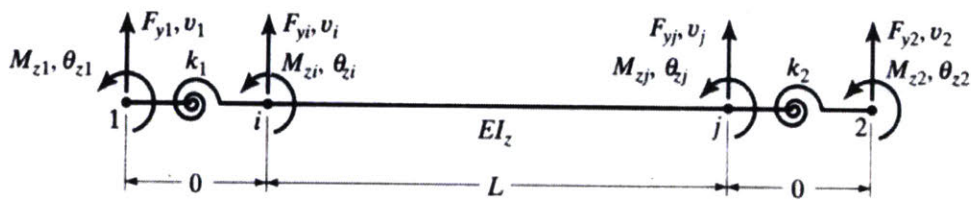


Figure 26-Modified beam element with rotational springs for the modeling of semi-rigid or flexible connections [53]

The stiffness of the rotational springs k can be calculated from the relationship $M = k\theta$ where M = transmitted moment with respect to θ and θ = the relative rotation between the two connected members [53]. By varying the stiffness k from $k = 0$ to $k = \infty$ rigid and flexible connections can

be modeled. The addition of the rotational springs results in a change of the stiffness matrix of the system, further details regarding the modified stiffness matrix can be found in reference [53]. In our case, an assumption of an ideally flexible connection is suitable, therefore where there is a non-zero stiffness value, the springs are set to a high value to approximate $k = \infty$. To reduce the likelihood of a badly conditioned matrix and thus inaccurate results, these high values are limited to the order of 10^{13} lb/in. The high stiffness limit is defined by the review of values used in literature for the same applications [4,53]. Zero length rotational springs to model the hinge conditions are added to all external nodes which connect one SLE unit to the other (Figure 27).

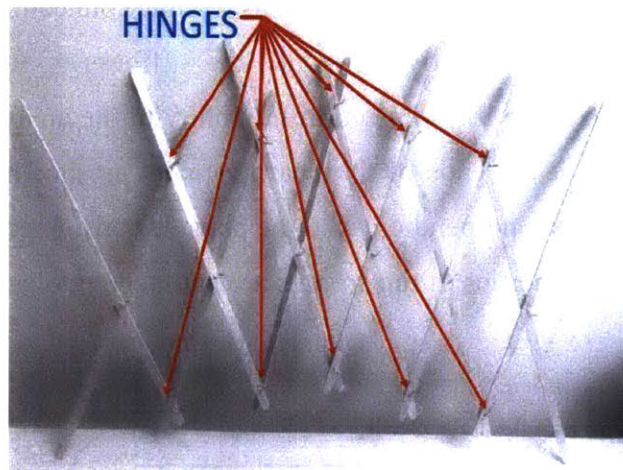


Figure 27- External hinge locations on coffee stirrer model of a rectilinear translational geometry $T(2)$ with an arch like pattern.

After the modification of the FEA, various approaches were used to demonstrate enrichment of the code. To check the flexible connections, results from models with and without internal hinges from our MATLAB implementation, Mastan [53] and hand calculations were compared for simple examples. The internal forces, bending moments and node deflections were checked. Additionally, to check the discrete beam elements and special connections, we modeled a comparative structure with the modified FEA code. Internal forces and bending moments of the model were compared to results calculated using the derived moment and force equations for SLE structures described in [3,37]. All calculations and models provided nearly identical results, thus confirming our static analysis.

Chapter 5 Results

5.1 Results

The SLE structure was subjected to an H15 live load as described in section 3.2. In order to determine the most critical load condition, the structure was analyzed with the point loads, spaced 14 ft from each other, in the locations shown in Figure 28.

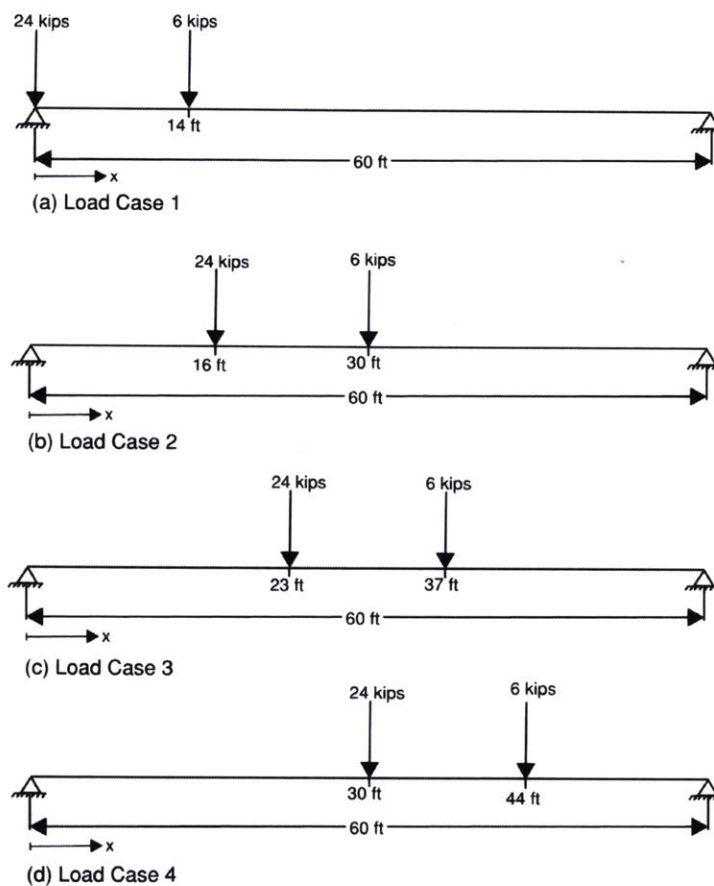


Figure 28-Live load locations. Load case #4 resulted in the most critical loading location, figure 28(d)

It was found that load case 4 (Figure 28d) generates the largest stresses and deflections on the system, thus defining the most critical load location. Consequently, this load case was used throughout the analysis for the sizing optimization and the comparative studies between the different geometries.

Following the design process outlined in section 3.1 a discrete number of cross section depth and thickness variables was selected. The initial design variables used were:

$$Depth (in) = \{12 \ 14 \ 16 \ 18 \ 20 \ 22 \ 24\}$$

$$Thickness (in) = \{1 \ 2 \ 3 \ 4\}$$

After the initial design and optimization, although the FEA converged satisfying equilibrium, most solutions obtained were very close to the highest limit of the variables provided. These resulted mostly in depths of 24 in and thicknesses of 3 or 4 in. Because of this, we decided to go back to the selection of variables and increase the number of options to include larger depth dimensions. The subsequent depth range provided was:

$$Depth (in) = \{18 \ 20 \ 22 \ 24 \ 26 \ 28 \ 30\}$$

The addition of larger depth dimensions led to more diverse solutions throughout the different geometries and deck depth cases. Once the selection of the discrete variables was determined, the geometric analysis and shape optimization were performed.

The objective function is dependent on the design angle at which the structure performs in service. Varying the angle θ_1 caused not only a change in the number of SLE units required for the specified span, but also a change in the performance of the structure, thus directly affecting the total weight.

After the analysis and summary of the data provided by several iterations of the GA, it was found that most geometries achieved the lowest weight solution at an angle $\theta_1 = 33^\circ$. Furthermore, the geometries at the optimal angles also resulted in the structures with the lowest stresses and bending moments. The resulting angles for the 5 defined bridge types described in Table 4 are listed in Table 5. Furthermore, relationships between the various deployed angles and corresponding total weight of the structures are shown below in Figure 29, Figure 30 and Figure 31 for the three considered SLE translational systems. For the purposes of this study, the total weight of the structure is defined as the weight of the two planar SLE lattices plus the weight of the bridge deck. The results show that there is no linear relationship between the objective function and θ_1 , however data clusters can be recognized. For $T(1)$ the heaviest structures are resultants of deployed angles between 34 to 39 degrees, and the lightest of angles from 24-33 and 40-44 degrees, with a substantial increase in the objective value when the structure reaches 45 degrees and beyond.

A very similar behavior is observed for $T(2)$ and $T(3)$ geometries. Furthermore, there is a significant increase in the solution values immediately after the angle at which the lowest weight solution is found.

Since multiple angles resulted in the lowest total weight, additional considerations such as internal forces were taken into account to select the overall most efficient solution at each configuration.

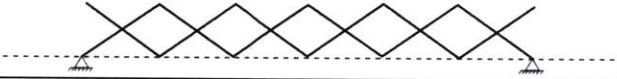




	Geometry	Resultant Deployed Angle, θ_1 (degrees)
T(1)-A		33
T(1)-B		31
T(2)-A		43
T(2)-B		33
T(3)-A		33

Table 5- Resultant deployed angle for the most optimal SLE structural performance per geometry as defined in section 4.2

Minimum Weight Solution for all Angles θ_1 in Design Domain for a $T(1)$ Geometry at Full and Mid-Depth Deck Locations

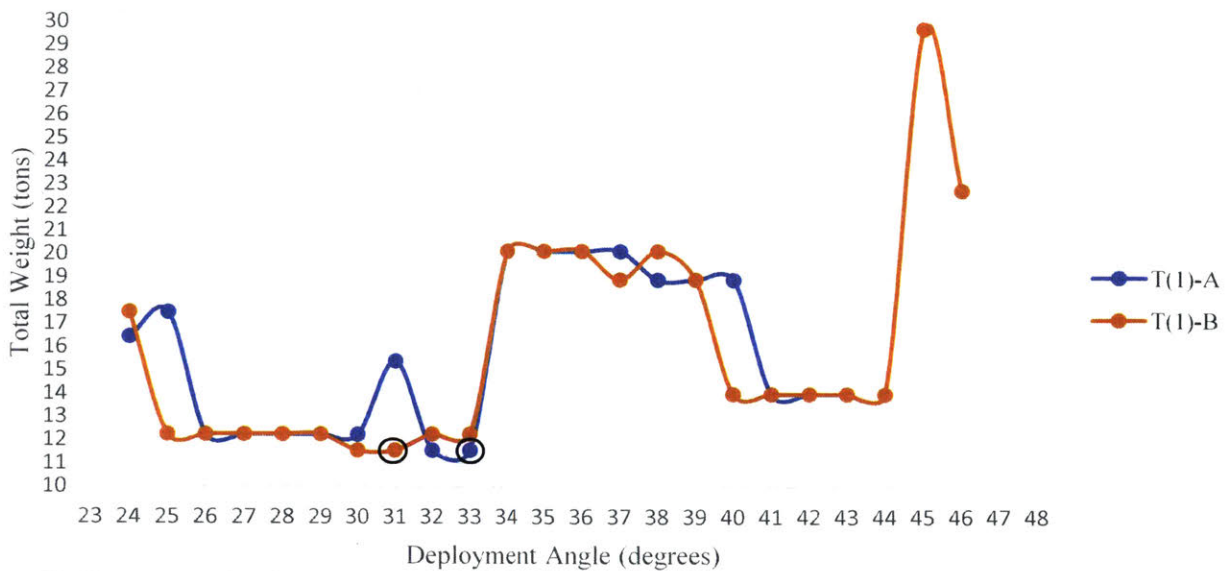


Figure 29-Minimum weight solutions for all angles θ_1 in design domain for a $T(1)$ geometry

Minimum Weight Solution for all Angles θ_1 in Design Domain for a $T(2)$ Geometry at Full and Mid-Depth Deck Locations

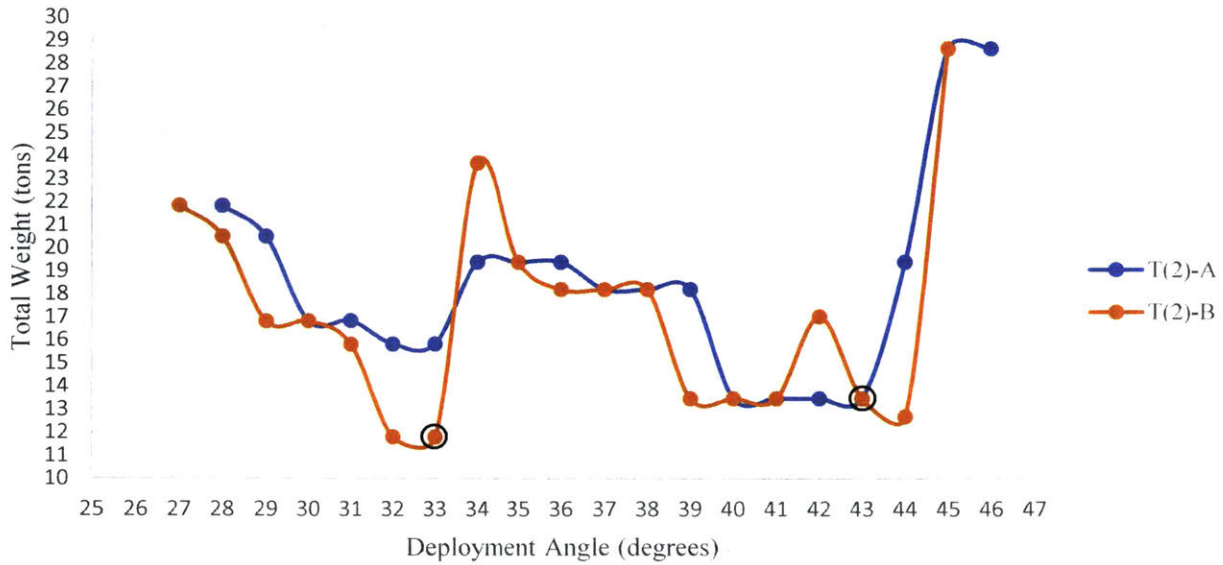


Figure 30-Minimum weight solutions for all angles θ_1 in design domain for a $T(2)$ geometry

Minimum Weight Solution for all Angles θ_1 in Design Domain for a $T(3)$ Geometry at a Mid-Depth Deck Location

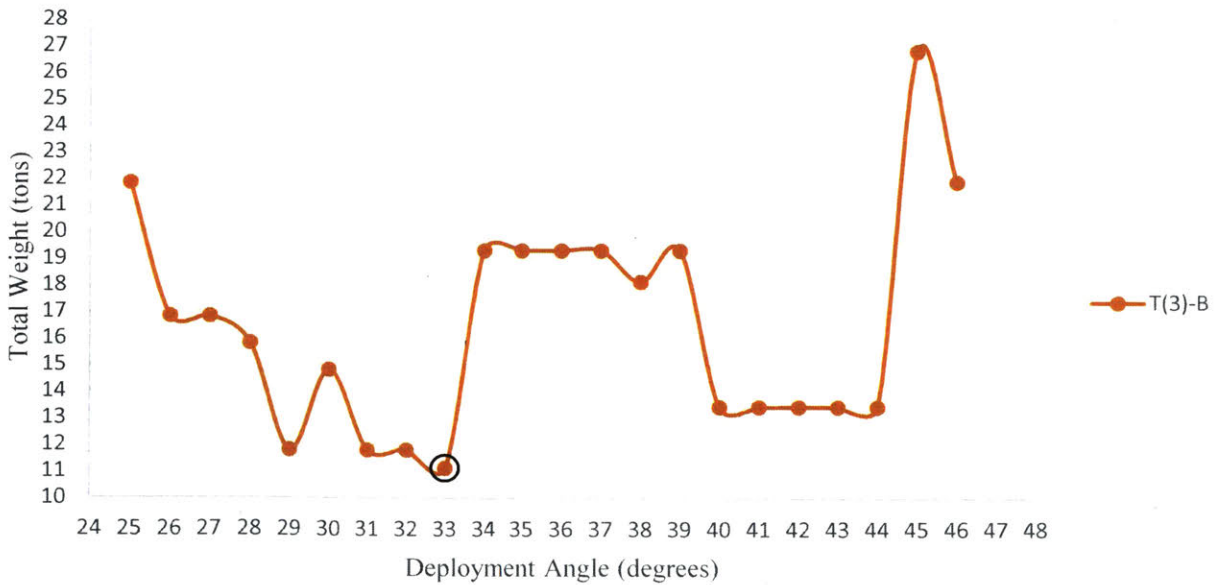


Figure 31-Minimum weight solutions for all angles θ_1 in design domain for a $T(3)$ geometry

Table 6 lists the lowest member area solutions and the objective function values for each bridge type at the selected deployed angles. The solutions for geometries $T(1)$ -A, $T(1)$ -B and $T(3)$ -B are the lowest sections with areas of 28 in x 2 in. Nonetheless, the rectilinear translational geometry with different member lengths $T(3)$ -B, resulted in the structure with the overall lowest total weight. In contrast, although similar, geometries $T(2)$ -A and $T(2)$ -B required a larger section with dimensions 30 in x 2 in, thus being the least efficient geometry for our design parameters.

Structure	Total number of SLE units	θ_1 (degrees)	Cross-Sectional Area (in ²)	Depth (in)	Thick-ness (in)	Weight (lbs)	Deck Weight (lbs)	Total Weight (lbs)	Total Weight (tons)
$T(1)$ -A	6	33	56	28	2	9803	3523	23128	11.56
$T(1)$ -B	6	31	56	28	2	9803	3601	23207	11.60
$T(2)$ -A	7	43	60	30	2	11743	3584	27070	13.54
$T(2)$ -B	6	33	60	30	2	10065	3523	23653	11.83
$T(3)$ -B	6	33	56	28	2	9394	3523	22312	11.16

Table 6-Lowest cross sectional area solutions and objective function values for all geometries

Based on the results obtained we can conclude that the geometry $T(3)$ -B at a deployed angle θ_1 of 33 degrees results is the most optimal configuration with respect to the objective function as defined herein (Figure 32). $T(3)$ -B provides the lightest SLE structure with a total weight of 11.16 tons, designed per the parameters and loading conditions presented in this paper while still meeting the constraints defined by AASHTO and a deflection limit of $S/400$.

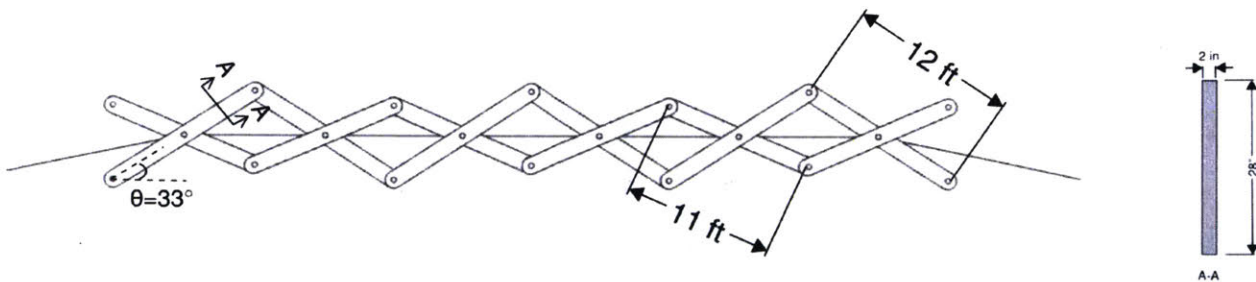


Figure 32- $T(3)$ -B Geometry. Most optimal result based on minimum weight optimization objective

Furthermore, the respective stresses, bending moments and deflections, together with the maximum allowable values per AASHTO are compared and tabulated in Table 7. From the results,

it can be concluded that the design is governed by deflection and that the deflection decreased as the weight of the structure increased, which is expected. The lowest weight solution and corresponding deflection for each of the geometries is plotted in a weight-deflection graph (Figure 33). Although the selected structure does not result in the lowest deflection, it is within 9% of the lowest value. Furthermore, it should also be noted that the structure with the lowest deflection $T(2)$ -A, has a considerably higher weight when compared to the others.

We can also conclude that the highest internal forces for all geometries are caused by the element bending moments. However, as shown in Figure 34 the bending moments do not show a direct correlation to the total weight of the structure. More so, it displays a relationship with the overall geometry. The $T(1)$ structures which have only a slight increase in weight compared to our selected structure $T(3)$, resulted in the lowest bending moments. However, the resultant moments for our proposed structure are within 13% of the lowest values. Considering our design objectives, we gave priority to the structure's weight when the difference in bending moments and deflections were small and still proposed the $T(3)$ -B structure as our concept design. Structure $T(3)$ -B results in internal forces and deflections which are well below the design constraints and are comparable to the other selected geometries. Yet, at the same time, it provides the lightest structure which results in an advantage for transportation and installation. Axial and shear forces are not significant when compared to the design constraints.

Structure	M_{e-max} (kip-in)	M_{allow} (kip-in)	C_{e-max} (kips)	C_{allow} (kips)	T_{e-max} (kips)	T_{allow} (kips)	V_{e-max} (kips)	V_{allow} (kips)	d_{nmax} (in)	d_{allow} (in)
$T(1)$ -A	2902	8794	-67	-1764	62	1751	40	1058	1.71	1.80
$T(1)$ -B	2702	8794	-57	-1764	62	1751	38	1058	1.72	1.80
$T(2)$ -A	2784	9422	-54	-1890	50	1877	42	1134	1.58	1.80
$T(2)$ -B	3142	9422	-70	-1890	66	1877	44	1134	1.65	1.80
$T(3)$ -B	3092	8794	-66	-1764	65	1751	43	1058	1.72	1.80

Table 7- Resultant forces and deflections for all selected geometries

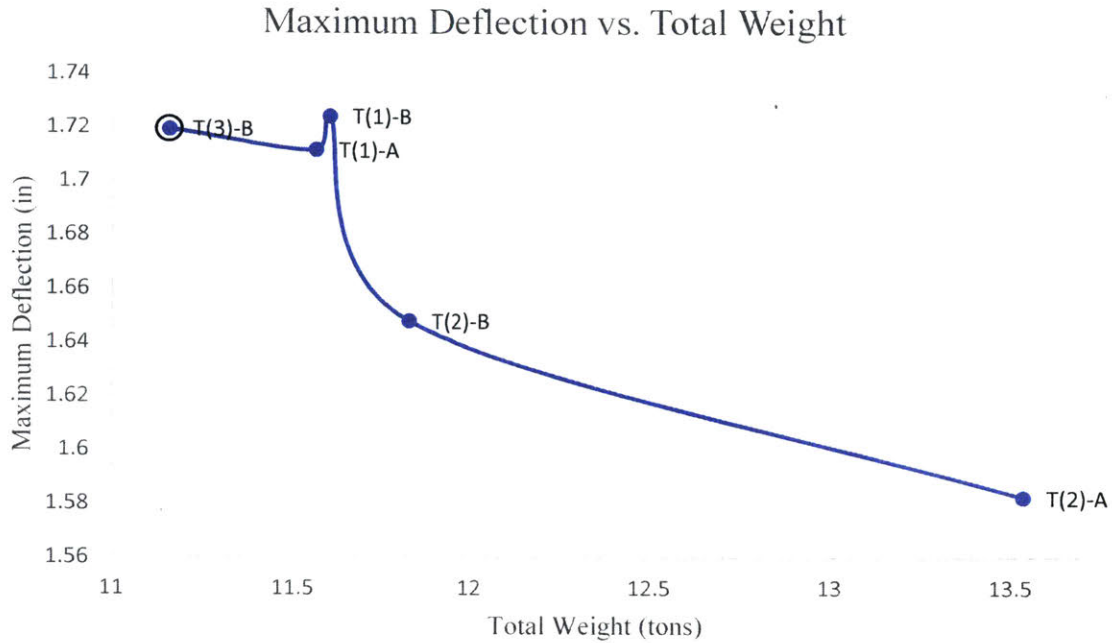


Figure 33-Maximum deflections vs. total weight relationship for the selected bridge geometries

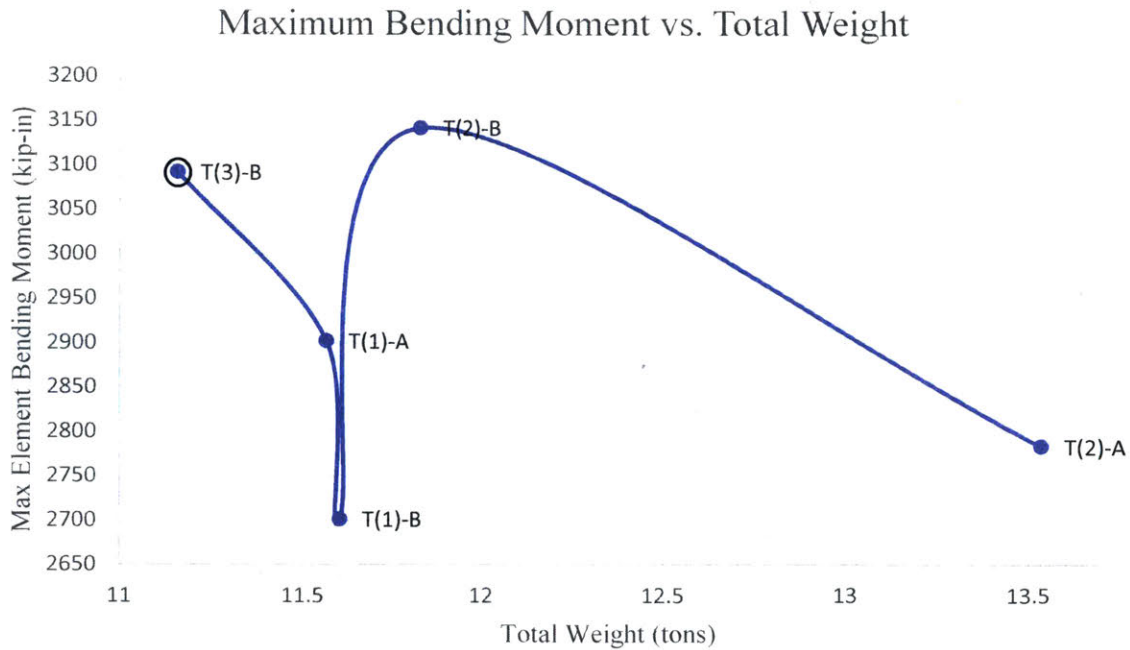


Figure 34-Maximum bending moments vs. total weight relationship for the selected bridge geometries

After the structures were designed at their deployed state, a deployment check was performed on the selected bridge geometries discussed above. Although we are most concerned with the selected structure *T(3)-B*, analysis for all optimal sections at the various geometries were computed for

comparison. As explained in section 3.2 we analyze the structure with a fix-fix and pin-pin condition. As expected, using a pin-pin cantilever condition further increased the deflection, however, only a relatively small difference is observed since the resulting deflection is increased 2-3.5%. Specifically, the use of pin connections for our selected geometry $T(3)$ -B only increased the maximum deflection by 2.66%. In this condition, the highest internal forces for all geometries are also the element bending moments. The resulting member stresses and maximum deflections are shown in Table 8.

Maximum Member Forces and Deflections During Deployment							
Structure	Support Condition	M_{e-max} (kip-in)	C_{e-m} (kips)	T_{e-max} (kips)	V_{e-m} (kips)	d_{n-max} (in)	Deflection increase from change in support condition (%)
$T(1)$ -A	Fix-fix	2780.6	-90.2	93.8	38.6	4.73	3.44
	Pin-pin	2780.6	-70.7	73.1	38.6	4.89	
$T(1)$ -B	Fix-fix	2585.1	-95.9	95.9	35.9	4.70	3.08
	Pin-pin	2585.1	-76.0	76.0	35.9	4.85	
$T(2)$ -A	Fix-fix	3262.6	-85.9	94.8	49.4	4.92	3.61
	Pin-pin	3262.6	-65.5	73.1	49.4	5.10	
$T(2)$ -B	Fix-fix	2857.9	-105.7	101.6	39.7	4.02	2.10
	Pin-pin	2857.9	-87.0	85.6	39.7	4.10	
$T(3)$ -B	Fix-fix	2902.9	-104.1	96.0	40.3	4.54	2.66
	Pin-pin	2902.9	-83.9	79.7	40.3	4.66	

Table 8-Maximum member forces and deflections under deployment support conditions at the critical location

Although the deflections during deployment surpass the deflection limit stipulated, the elements in the structure are still below the allowable stresses and bending moments. Additionally, during deployment, our main concern regarding deflection is that the structure lands in elevation with the supports. Studying precedents of deployed structures and considering military deflections limits of $S/100$ [45], we can argue that the structure would satisfy this condition without requiring additional strengthening. Furthermore, if decreasing the deflection during deployment is of concern, different means of construction can be further studied to compensate and decrease the resulting deflection. For example, if available during installation, the structure may be installed

using heavy equipment such as a crane. The crane can provide an additional support point therefore changing the structure's support condition and decreasing the cantilever length.

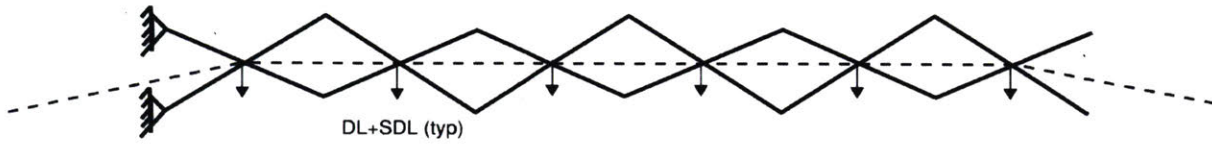


Figure 35-Supports and loading schematic for deployability check of the structure for pin-pin connection cantilever option

Although we can expect the critical element forces during deployment to occur when the bridge is closest to its final deployed position, the structure was checked at all stages of deployment for validation. The results, which are plotted below (Figure 36, Figure 37), confirmed our assumptions. As the bridge is being extended the internal forces increase, therefore reaching the maximum deployment stresses when the structure is closest to its full extension.

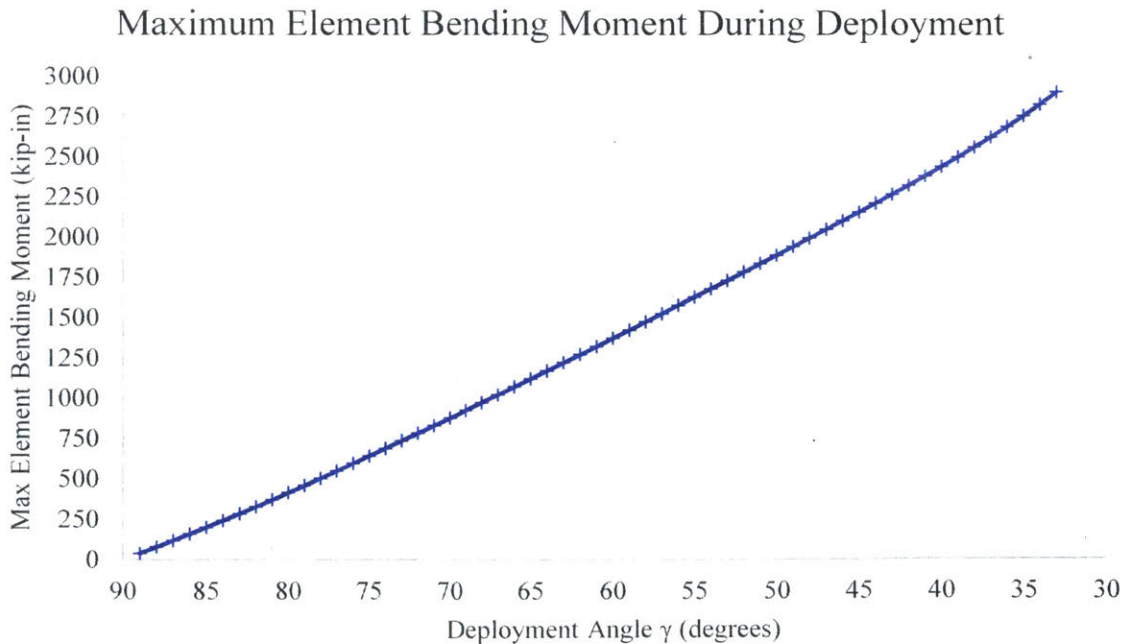


Figure 36-Element bending moment during deployment for the T(3)-B bridge configuration

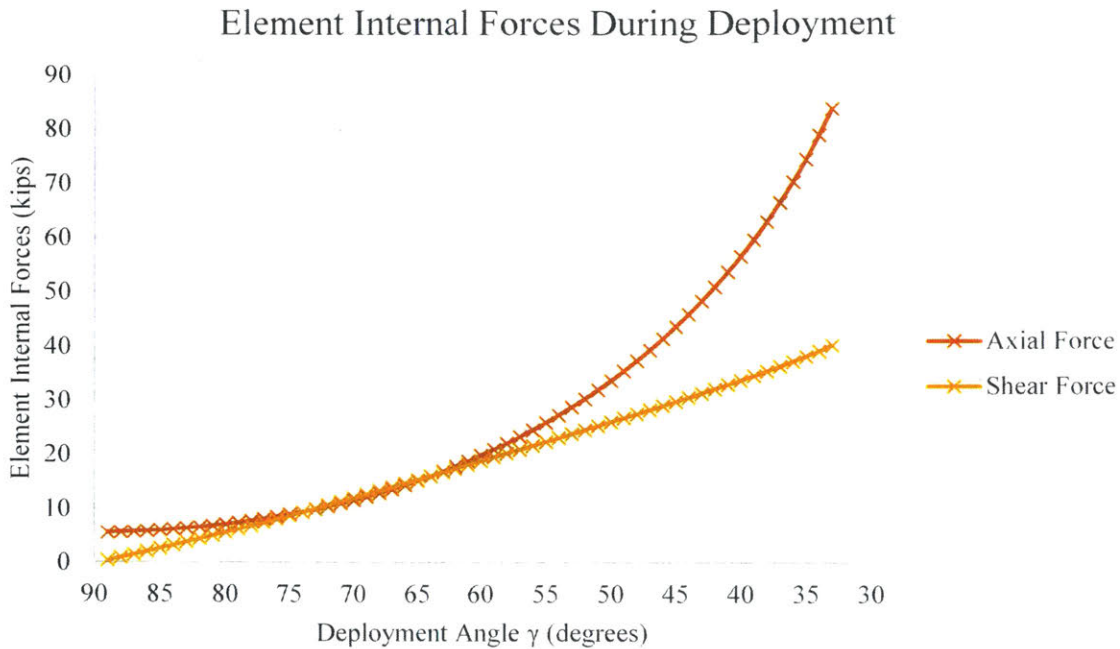


Figure 37-Element internal forces during deployment for the T(3)-B bridge configuration

For post processing and to further compare the optimality of our design, we explored a wider design domain by incorporating the length of the rigid bar d_2 , as a variable for our optimization problem, which was initially set up as constant length of 11 ft. The length was allowed to vary from 10 ft up to 12 ft in discrete increments of 0.1 ft. The best results per design length are plotted below in a length-total weight graph (Figure 38). The optimal design angles, varied by the change in member lengths, and are displayed as data point labels. After an analysis of the data, the best solution with respect to our problem was still the proposed solution described above with a member length of 11 ft and angle of 33 degrees. At a member length shorter than 11 ft, although structural equilibrium was still achieved, the optimal solution had deployed angles larger than those in our current results. Consequently, additional SLE units were required to cover the span length which increased the total weight of the structure. This evaluation confirmed our results.

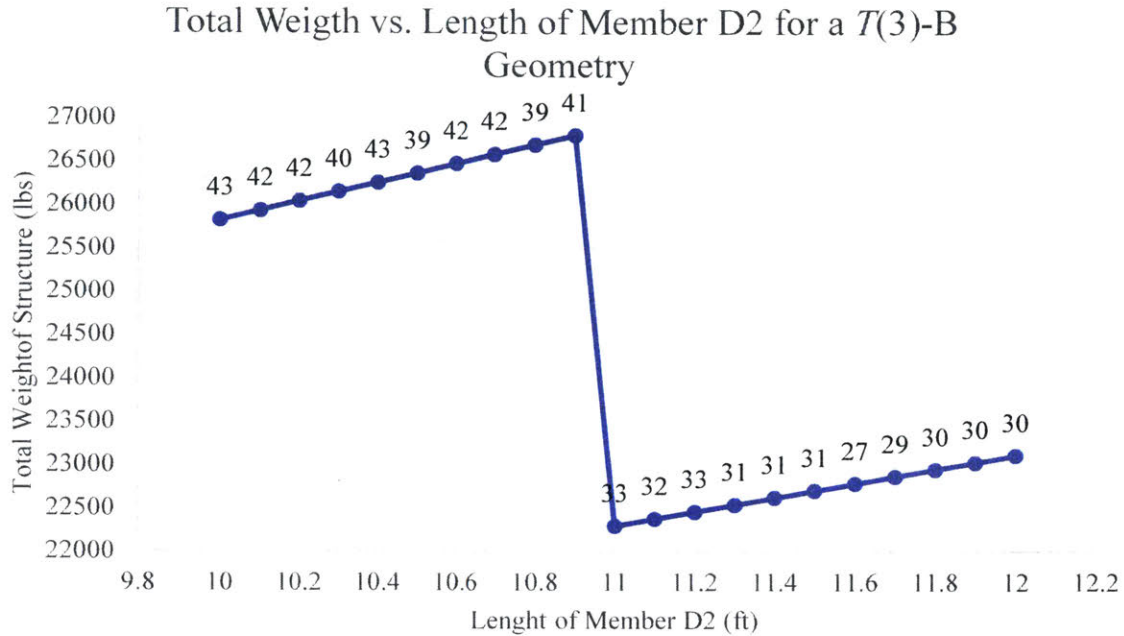


Figure 38-Problem solutions based on variable member length and deploy angle for a T(3)-B geometric configuration

5.2 Discussion

From our analysis we can conclude that the geometry of a deployable SLE structure plays a very important part on its performance and thus the design objective. The shape optimization solutions varied significantly depending on the deployed angles, deck depth location and SLE system geometries. Nonetheless, even when the optimal cross-sectional areas were equal across geometries, the difference in member lengths, which characterize geometries $T(2)$ and $T(3)$, caused a further reduction in the function values. As a result, geometry $T(3)$ -B at a deployed angle of 33 degrees and a cross sectional area of 56 in^2 provides the overall best solution with a function value of 11.16 tons.

The data clusters recorded in the angle vs. weight plots confirm that the number of SLE units has an effect on the performance of the structure. For all geometries, the structure requires an additional SLE unit for $\theta_1 \geq 34^\circ$, at which point the data shows a noticeable weight gain. This gain is not only due to the additional unit but also, when $34^\circ < \theta_1 \leq 39^\circ$, the structure requires a larger cross sectional area to meet the design constraints. However, at approximately $40 \leq \theta_1 < 45^\circ$ the system performs better resulting in a lower required cross sectional area, and consequently

lower total weight. This behavior can be seen again once the structure reaches at $45 \leq \theta_1$ when an additional SLE unit is required thus destabilizing the system.

Furthermore, it was also found that in most cases, changing the location of the deck resulted in different solutions. Over 75% of the cases had equal or better solutions when the bridge was modeled as a half through bridge. More specifically, while discussing the selected structures, geometry $T(1)$ resulted in the same optimal member sizes for both conditions, however, the stresses of the members decreased when the structure was a half through bridge. In geometry $T(2)$ the location of the deck influenced the structure substantially, for which the half through bridge resulted in a better solution. The $T(2)$ through bridge structure required an additional SLE unit to meet the span length since its optimal deployed angle was larger, thus increasing the total weight. Nonetheless, a 3D analysis needs to be done to ensure transverse bars at the top of the structure are not required, thus still providing the vertical clearance while using a half through bridge.

The proposed design is still in the conceptual phase and was idealized to provide a basis for further design and detailing. Significantly more research and structural design considerations need to be incorporated into the work such as friction in the connections, discrete joint dimensions and lateral forces. Moreover, considering the thin member sizes, buckling becomes an important design consideration which must be accounted for.

Our design proposes a bridge structure which is comparable to published designs found in literature. Compared to the Mobile Bridge 4 [31], our current SLE bridge design has a lighter weight per unit length. Furthermore, considering our design is an idealized design in the conceptual stages, and therefore adding 15% weight for added components, the study still provides a system which, based on its objective function, is a better solution. Compared to the Medium Girder Bridge [21], our proposed structure weighs approximate 18% more. However, the MBG is a modular structure which requires onsite connections, whereas our bridge is deployable.

Table 9 lists some of the main parameters for the proposed design structure compared to two bridge structures presented in literature and briefly discussed in section 2.1 and 2.2 respectively [21,31].

Bridge Type	Single Story Medium Girder Bridge [21]	Proposed Bridge Design	MB4 [31]
Carrying Capacity	MLC 20≈20 Tons	15 Tons	4.5 Tons per Unit
Length	62.34 ft	60.38 ft	68.24 ft
Weight	9.5 Tons	11.16 Tons	130 kN≈14.62 Tons
Weight per foot	304.78 lbs./ft	369.66 lbs./ft	428.5 lbs./ft

Table 9-Design comparison with existing bridge designs. [21,31]

The bridge design currently does not meet the allowable deflections set by AASHTO. However, additional considerations are being incorporated to improve the stiffness, without compromising the deployment capabilities of the structure. This includes the addition of horizontal members which would be attached to the diagonal beams when the structure is folded, and would extend and self-lock horizontally when in service (Figure 39). These members would serve a dual purpose, to increase the stiffness as well as to lock the structure in place at the design angle. The members are proposed to not be coplanar with the bars to avoid affecting the foldability of the system.

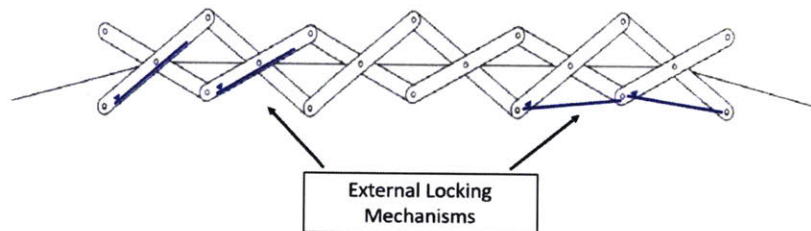


Figure 39-Conceptual proposal for external locking mechanisms. SLE units on the left show the proposed locking member configuration in the folded position, whereas units on the right show locking members on their final deployed position.

Nonetheless, a defined deflection limit specific to the field of temporary, deployable structures could potentially encourage less conservative designs while efficiently satisfying the requirements of their specific application.

Furthermore, even though the bridge does not have the same loading capacity as some of the existing modular bridges, it proposes a design with the advantage of not requiring onsite connection of modules. This advantage, together with the light weight design, are important considerations in the context of disaster relief since under these events, the probability of lack of resources is higher. Therefore, providing a system which would require less force and labor for installation, can potentially aid in expediting the communities' resilience by allowing available resources to be allocated to other relief efforts.

Chapter 6 Conclusion

6.1 Summary of Findings

In this thesis we proposed a structural design for a deployable bridge structure composed of SLE translational units. The design problem was defined as an optimization problem for minimum weight subjected to stress limits defined by AASHTO [19] and to deflection limits specified herein. The deflection limits were defined as half the difference between the AASHTO limits and the limits used for temporary bridge design in literature as described in section 4.4. The optimization problem was solved for different known scissor like element (SLE) deployable geometries which are compared to each other to find the best solution.

We found that the best geometry with respect to the objective function is composed of an asymmetric SLE unit that is mirrored along its unit line (defined as $T(3)$ herein) with a half through deck location and a deployed angle of 33 degrees. Additionally, the rigid bars which compose the SLE unit are of 11 ft and 12 ft in length. For this configuration the minimum cross section required to meet the design constraints within the defined domain is a 28 in x 2 in rectangular member.

When compared to the existing Mobile Bridge V4 (described in detail in chapter 2), our proposed SLE bridge design weights approximately 14% less per unit length. When compared to the MGB (described in Table 1) our proposed structure weighs approximate 18% more per unit length. However, the MGB is a modular structure which requires onsite connections, whereas our bridge is extendible.

This study provides a system which, based on the minimum weight objective function, is a competitive solution for the proposed application. Given the potential lack of resources after a natural disaster, providing a light weight, easily transportable, extendible structure which requires less force and resources for installation, can have a positive impact in the recovery process.

6.2 Future Work

This research is still in the conceptual phase, additional design considerations must be further studied and incorporated in the design results. These include, the effects of friction in the connections, discrete joint dimensions and lateral forces. Furthermore, as the selected sections have narrow cross sectional areas, buckling might become an important parameter which should be accounted for. In addition, further research should also focus on the potential need for longer approaches due to the change in elevation required to reach the deck location and on a 3D analysis to ensure transverse bars at the top of the structure are not necessary.

Nonetheless, the presented research demonstrates that restraining the design with constant member lengths and cross sectional areas may result in solutions which use more material than required to meet the problem constraints. Based on this, we can argue that further weight minimization could be done by extending the design domain to include variable element topologies and cross-sectional areas along the members. Hence, allowing optimization results which would only use enough materials to efficiently meet the design constraints.

References

- [1] US Bridge, Puerto Rico Hurricane Damage Coverage – US Bridge To Build 4 Bridges, retrieved May 7 2018 from: <<https://usbridge.com/puerto-rico-hurricane-damage-4-new-bridges/>>
- [2] M. Saatcioglu, A. Ghobarah, I. Nistor, Performance of Structures in Indonesia during the December 2004 Great Sumatra Earthquake and Indian Ocean Tsunami, *Earthquake Spectra*, vol. 22, no.3, 2006, pp. 295-319.
- [3] Y.Chikahiro, I. Ario, M. Nakazawa, Theory and Design Study of a Full-Scale Scissors-Type Bridge, *Journal of Bridge Engineering*, vol. 21, no.9, 2016.
- [4] Structurae, New Po River Bridge, retrieved April 12 2018 from: <<https://structurae.net/structures/new-po-river-bridge>>
- [5] J.C. de la Llera, F. Rivera, J. Mitrani-Reiser, R. Junemann, C. Fortuno, M. Rios, M. Hube1, H. Santa Maria, R. Cienfuegos, Data Collection After the 2010 Maule Earthquake in Chile, *Bull Earthquake Eng.* vol.15, 2017, pp.555–588.
- [6] U.S. Department of Transportation, Department of Transportation Awards \$40 Million to Puerto Rico for Emergency Road and Bridge Repairs, retrieved April 1 2018 from: <<https://www.transportation.gov/briefing-room/departement-transportation-awards-40-million-puerto-rico-emergency-road-and-bridge>>
- [7] The Columbian, Floods in Southern Japan Force Hundreds to Flee; 2 dead, retrieved April 1 2018 from: <<http://www.columbian.com/news/2017/jul/06/floods-in-southern-japan-force-hundreds-to-flee-2-dead/>>
- [8] B.R. Russell, A.P. Thrall, Portable and Rapidly Deployable Bridges: Historical Perspective and Recent Technology Developments, *Journal of Bridge Engineering*, vol. 18, no.10, 2013, pp.1074-1085.
- [9] E.J. Gerbo, C.M. Casias, A.P. Thrall, T.P. Zoli, New Bridge Forms Composed of Modular Bridge Panels, *Journal of Bridge Engineering*, vol.21, no.4, 2016, 04015084.
- [10] Y.Wang, A.P. Thrall, T.P. Zoli, Adjustable Module for Variable Depth Steel Arch Bridges, *Journal Constructional Steel Research*, vol. 126, 2016, pp. 163–173.
- [11] C.H. Hernandez Merchan, Deployable Structures, Master’s Thesis Department of Architecture, Massachusetts Institute of Technology, Cambridge, Massachusetts, 1987.
- [12] Vectorstock, Umbrella Open and Close Vector Image, retrieved May 8 2018 from: <<https://www.vectorstock.com/royalty-free-vector/umbrella-open-and-closed-vector-937689>>

- [13] C.J. Gantes, *Deployable Structures: Analysis and Design*, WIT Press, 2001.
- [14] L. Alegria Mira, N. De Temmerman, C. Preisinger,. *Structural Optimisation of Deployable Scissor Structures Using New Computational Methods.*, *WIT transactions on the built environment*, vol. 124, 2012, pp. 469–480.
- [15] L. Alegria Mira, R. F. Coelho, A.P. Thrall, N. De Temmerman, *Parametric Evaluation of Deployable Scissor Arches*, *Engineering Structures*, vol. 99, 2015, pp. 479–491.
- [16] S. Pellegrino, *Deployable Structures*, Springer-Verlag Wien New York, 2001.
- [17] A. Hanaor, R. Levy, *Evaluations of Deployable Structures for Space Enclosures*, *International Journal of Space Structures*, vol. 16, no. 4, 2001, pp. 211-229.
- [18] N. De Temmerman, *Design and Analysis of Deployable Bar Structures for Mobile Architectural Applications*, PhD dissertation, Department of Architectural Engineering Sciences, Vrije Universiteit Brussel, Brussels, Belgium, 2007.
- [19] AASHTO, *Load and Resistance Factor Design (LRFD) Bridge Design Specifications: Customary U.S. units*, 7th Ed., 2014 Washington, DC.
- [20] U.S. Department of the Army. *Combined Arms Gap-Crossing Operations Field Manual 3-90.12.*, MCWP 3-17.1 (FM 90-13), 2008.
- [21] WFEL, *MGB Technical Specification*, retrieved march 15 2108 from: <<https://www.wfel.com/products/medium-girder-bridge/4/specification>>
- [22] Bailey Bridges, Inc., *The Bailey System*, retrieved May 5 2018 from: <<http://www.baileybridge.com/>>
- [23] Acrow, Rentals, retrieved March 15 2018 from: < <https://www.acrow.com/products-services/bridges/details/#temporary>>
- [24] Mabey, *Temporary Steel Bridge Overview*, retrieved March 15 2018 from: <Temporary Steel Bridge Overview>
- [25] Leonardo DRS, *Joint Assault Bridge (JAB)*, retrieved March 15 2018 from: <<http://www.leonardodrs.com/products-and-services/joint-assault-bridge-jab/>>
- [26] Aegistechnologies, *Why Did the Tank Cross the Road?*, retrieved March 15 2018 from: < <https://aegistg.com/why-did-the-tank-cross-the-road/>>
- [27] WFEL, *Dry Support Bridge*, retrieved March 15 2018 from: <<https://www.wfel.com/products/dry-support-bridge/5WFEL.com>>

- [28] A. Tugilimana, A.P. Thrall, R. F. Coelho, Conceptual Design of Modular Bridges Including Layout Optimization and Component Reusability, *Journal of Bridge Engineering*, vol.22, no.11, 2017, 04017094.
- [29] G. Lederman , Z. You, Branko Glisic, A Novel Deployable Tied Arch Bridge, *Engineering Structures*, vol.70, 2014, pp. 1–10.
- [30] I. Ario, M. Nakazawa, Y. Tanaka, I. Tanikura, S. Ono, Development of a Prototype Deployable Bridge Based on Origami Skill, *Automation in Construction*, vol. 32, 2013, pp. 104-111.
- [31] Y. Chikahiroa, I.Ariob, P. Pawlowskic, C. Graczykowskic, M. Nakazawad, J. Holnicki-Szulcc, S. Ono, Dynamics of a Scissor Type Mobile Bridge. X International Conference on Structural Dynamics, *Procedia Engineering*, (EURODYN 2017), vol. 199, 2017, pp. 2919–2924.
- [32] F. Yeh, K. Chang, Y. Sung, H. Hung, C. Chou, A Novel Composite Bridge for Emergency Disaster Relief: Concept and Verification, *Composite Structures*, vol. 127, 2015, pp. 199–210.
- [33] G. R. Thomas, B. J. Sia, A Rapidly Deployable Bridge System, *Structures Congress 2013*, 2013, pp. 656-667.
- [34] G. Sedlacek and H. Trumpf, Development of a Light-Weight Emergency Bridge, *International Conference on High Performance Materials in Bridges*, 2003, pp. 150-161.
- [35] M. J. Robinson, P.E.1, J. B. Kosmatka, P.E, Development of a Short-Span Fiber-Reinforced Composite Bridge for Emergency Response and Military Applications, *Journal of Bridge Engineering*, vol.13, no.4, 2008, pp. 388-397.
- [36] R. G. Wight, M. A. Erki, C. T. Shyu, R. Tanovic, P. J. Heffernan, Development of FRP Short-Span Deployable Bridge—Experimental Results. *Journal of Bridge Engineering*, vol.11, no.4, 2006, pp.489-498.
- [37] F. Escrig, Expandable Space Structures. *Journal of Space Structures*.,vol 1, no.2, 1985, pp.79–91.
- [38] F. Maden, K. Korkmaz, Y. Akgün, A Review of Planar Scissor Structural Mechanisms: Geometric Principles and Design Methods, *Architectural Science Review*, vol. 54, no. 3, 2011, pp. 246-257.
- [39] C.J. Gantes, P. G. Georgiou, V. K. Koumoussis, Optimum Design of Deployable Structures Using Genetic Algorithms, *Computational Methods for Smart Structures and Materials*, WIT Press, 1998, pp. 255-264.

- [40] Z. You, S. Pellegrino. Foldable Bar Structures, *International Journal of Solids and Structures*, vol. 34, no. 15, 1997, pp. 1825–1847.
- [41] A.P. Thrall, M. Zhu, J.K. Guest, I. Paya-Zaforteza, S. Adriaenssens, Structural Optimization of Deploying Structures Composed of Linkages. *Journal of Computing in Civil Engineering*, vol. 28, no.3, 2014, 04014010.
- [42] L. Alegria Mira, A.P. Thrall, N. De Temmerman, The Universal Scissor Component: Optimization of a Reconfigurable Component for Deployable Scissor Structures. *Engineering Optimization*, 2015, pp. 1–17.
- [43] K. Roovers, N. De Temmerman, Digital Design of Deployable Scissor Grids Based on Circle Packing, *Proceedings of the International Association for Shell and Spatial Structures (IASS) Symposium 2015, Amsterdam*, 2015.
- [44] K. Roovers, N. De Temmerman, Deployable Scissor Grids Consisting of Translational Units, *International Journal of Solids and Structures*, vol. 121, 2017, pp. 45–61.
- [45] J.P. Hanus, L.C. Bank, J.C. Ray, G.I. Velazquez, *Optimized Design and Testing of a Prototype Military Bridge System for Rapid in-Theater Construction*, Engineer Research and Development Center, MS, 2006.
- [46] U.S. Department of Transportation Federal Highway Administration, Vertical Clearance, retrieved April 9 2018 from: <https://safety.fhwa.dot.gov/geometric/pubs/mitigationstrategies/chapter3/3_verticalclearance.cfm>
- [47] Landstar, Over-Sized & Heavy Freight / Specialized Services, retrieved April 9 2018 from: <<http://americasbesttrucking.com/landstar-specialized-heavy-haul>>
- [48] AASHTO Standard Specifications for Highway Bridges, Customary U.S. units, 17th Edition, 2002, Washington, D.C.
- [49] Belgard, Pavers Designed to Handle H-20/HS-20 Loading, retrieved April 9 2018 from: <http://www.belgardcommercial.com/resources/design_solutions/handles_h-20hs-20_loading>
- [50] MATLAB and Statistics Toolbox Release R2017b, The MathWorks, Inc., Natick, Massachusetts, United States.
- [51] J.S. Arora, *Introduction to Optimum Design*, 3rd Edition, Academic Press, 2012.
- [52] J.J. Munoz Romero, *Finite-Element Analysis of Flexible Mechanisms Using the Master-Slave Approach with Emphasis on the Modelling of Joints*, PhD Dissertation, Department of Aeronautics Imperial College London, UK, 2004.
- [53] W.McGuire, R.H. Gallagher, R.D.Ziemian, *Matrix Method of Structural Analysis*, 2 edition, Wiley, 1999.